

A Novel Analytical Approach for Axial Load Capacity Evaluation of Stiffened Hollow Steel Columns Utilizing Finite Element Method

Ezzaat A. Sallam¹, Ebrahim. Makled^{2*}, Mohamed Elghandour³, Ashraf Elsabbagh⁴

¹ Lecturer, Faculty of Engineering, Civil Engineering Department, Port Said University, Email: Ezzat.sallam@eng.psu.edu.eg

² Master Student, Faculty of Engineering, Civil Engineering Department, Port Said University, Email: ebrahimmakled4444@gmail.com

³ Professor, Faculty of Engineering, Civil Engineering Department, Port Said University, E-mail: dr.elghandor@gmail.com

⁴ Assistant Professor, Faculty of Engineering, Civil Engineering Department, Port Said University, Email: ashraf_ims@yahoo.com

*Corresponding author, DOI: 10.21608/PSEERJ.2023.199207.1225

Received 10-3-2023

Revised 19-7-2023

Accepted 27-7-2023

© 2023 by Author(s) and PSEERJ.

This is an open access article licensed under the terms of the Creative Commons Attribution International License (CC BY 4.0).

<http://creativecommons.org/licenses/by/4.0/>



ABSTRACT

This study presents a finite element (FE) investigation of stiffened and unstiffened box hollow columns having compact, non-compact and slender cross-sections for short as well as long columns. The available analytical methods neglected the effect of stiffener's length when calculating stiffened hollow steel sections axial capacity. Therefore, an extensive study was conducted on the effect of stiffener length on ultimate capacity of hollow steel columns. Also, the effect of different numbers of stiffeners on ultimate capacity of steel columns considering five different grades of steel was numerically studied using nonlinear finite element analysis. A nonlinear (FE) analysis of steel columns which accounts the effects of residual stresses and initial local and global imperfections in long columns was performed. The current FEM results and the analytical methods such as effective width equations were compared and discussed. The FE models built in this study is verified against the available experimental data under axial compression and showed good agreement. The stiffeners remarkably increases the ultimate capacity of slender sections in the long columns. As a major result of the conducted analysis taking into account the studied parameters, a novel equation was proposed to predict the ultimate capacity of box steel sections.

Keywords: Local buckling, Stiffened hollow square sections, Nonlinear analysis, Slender hollow square columns, Stiffener length.

1 INTRODUCTION

In industrial buildings, square hollow steel columns are regularly utilized, but they are employed more regularly in supporting structures for bridge design. These columns are produced in stiffened and unstiffened box hollow columns having compact, non-compact and slender cross sections. The global and local buckling are two different buckling modes that can occur in compression steel elements. The primary effect of local and global buckling is a reduction of the stiffening and

loading capacity of the member. The local and global buckling mode is significant affected by the ratio B/t ratio, the slenderness ratio L_e/r , and boundary conditions of the member. Where the L_e is the columns length, r is the radius of gyration, B is the columns width, and t is columns thickness. The initial imperfections, residual stress, and boundary conditions are critical factors in determining the ultimate strength of square hollow steel columns in compression members [1].

Many investigations on the behavior of square hollow steel columns have been conducted in the recent decades.

The stiffened and unstiffened square hollow columns (SHC), rectangular hollow columns (RHC) were investigated by Tao et al. [2]. The stiffened square hollow columns have only two longitudinal stiffeners welded to its longer sides as opposed to the four longitudinal stiffeners that were once present on each side of the stiffened square hollow columns (SHC). One of the most important considerations was the ratio (B/t). The tubes also come with or without stiffeners and the ultimate capacity of the experimental test results were presented. A comparative experimental test study between unstiffened and stiffened stainless steel hollow columns was presented by Dabaon et al. [3]. The ratio of length-to-depth (L/B) was fixed at a value of 3, but the depth-to-thickness ratio fluctuated from 60 to 90. For stiffened and unstiffened sections, the ultimate capacity of these columns, buckling modes, and axial load verses axial strain are compared. Somodi and Kövesdi [4] focused on the experimental measurements of the residual stress on welded box steel hollow columns with different steel grades and different B/t ratios. The aim of this investigation is to estimate the residual stresses, to determine the maximum compressive and tensile residual stresses. The experimental tests and finite element (FE) method of hollow long steel columns with non-compact and compact unstiffened sections were developed by Khan et al. [5]. The experimental test results concluded that the non-compact sections with $L_e/r > 24$ collapsed as a consequence of the combination of global and local buckling. Moreover, the compact cross-sections having L_e/r values between 35 to 109 collapsed in accordance with global buckling. According to the test data of estimation of slender non-compact box sections, it is necessary take into account that the reduction factor resulting from the global and local buckling effects. Javidan et al. [6] studied the behavior and ultimate capacity of an innovative steel hollow long column. The suggested innovative columns are made of mild steel plates that are joined at the corners to mild steel tubes. According to the test and FE modeling, a special focus is given to the effect of fabrication initial imperfections, residual stresses, and welding methods on the behavior of the suggested long hollow columns. Because of the compatibility between the steel plates and tubes in the column, the studied innovative steel hollow column specimens are demonstrated to have excellent compressive behavior, which significantly increases their capacity and ductility. El-Sayed et al. [7] presented a novel polymer-mortar system that strengthened square hollow columns, improving their behavior and capacity. For the square hollow short columns strengthened using polymer-mortar layer with the thickness equal to 6 mm, a maximum axial capacity improvement of 31.6% was achieved. For long columns, a polymer-mortar layer applied in 6 mm thickness on all four sides resulted in an ultimate capacity gain of 76.7%. Zheng et al. [8] studied the impacts of cold-forming in the behavior of stainless steel cold-formed hollow steel tube columns. In this

investigation a total of 19 and 32 specimens were tested for short and long columns, respectively. The buckling modes of the experimental specimens included the global buckling, local buckling, local-global buckling, and material strain hardening after yielding. The experimental test specimens collapsed in four different modes: global, local, both local-global, and plastic strength after yielding. Cold-formed hollow columns made of lean duplex stainless steel (LDSS) were designed and demonstrated by Anbarasu and Ashraf [9]. These columns that mainly collapsed due to the interaction of flexural and local buckling modes. In this study, the geometric parameters of the (LDSS) hollow column sections were selected so that the local and global buckling stresses are almost equal. Nassirnia et al. [10] developed a novel hollow columns made of ultra-high-strength steel tubes and corrugated plates. The corrugated plates that make up the suggested novel produced columns are welded to ultra-high strength (UHS) steel tubes and have a yield stress of $f_y = 1250 \text{ MPa}$ at the edges. The results demonstrated that the suggested novel columns are very efficient and ductile under axial compression load.

The finite element (FE) investigation of the fixed ended LDSS slender hollow columns with square (SHC), and non-regular hollow columns (NRHCs) was developed by Patton and Singh [11]. The non-regular hollow columns (NRHCs) such as L- (LHC) and T- (THC) shaped cross-sections. The Abaqus software was used to create the finite element (FE) models that was conducted under pure axial compression. The finite element results of square hollow columns and non-regular hollow columns were then compared with the design equations by the ASCE 8-02 and EN1993-1-4 requirements. The finite element results and code predictions have been demonstrated to agree significantly. Schillo and Feldmann [12] investigated both global and local buckling modes of the steel square hollow columns. The experiments were verified with the FE using Ansys software. The research presents an analytical method for determining a reduction factor that depends on slenderness. The finite element modeling of experimental tests on slender square hollow columns, subject to combined global and local buckling of steel plates was developed by Pavlovic et al. [13]. The parametric investigation used in the FE analysis are the influence of different imperfections, the cross-section geometry for cold-formed and welded columns, and the columns length. According to the results of a study, the initial imperfection can reduce resistance by up to 45% compared with perfect column.

The nonlinear finite element (FE) analysis of the square hollow stiffened and unstiffened high strength stainless steel (HSS) columns was developed by Ellobody [14]. The columns ultimate capacities, the axial load-shortening curves, and the collapse modes were predicted for the unstiffened and stiffened columns. The

main objective of this study was to investigate the effects of various section geometries on the columns capacity. Hilo et al. [15] studied the FE analysis on the ultimate capacity and behavior of polygonal hollow steel tube columns under axial compression load. In this investigation, different cross sections, including rectangular, circular, square, pentagonal, and hexagonal ones, have been provided. The finite element models have been analyzed to find the effect of the different cross-section shape, thickness, and length on the axial load behavior of the polygonal hollow steel tube columns. The FE analysis on the ultimate capacity and behavior of cold-formed steel rectangular and square hollow columns with two opposing circular holes in the center, at the height of the column was studied by Singh et al. [16]. The parametric analysis has been carried out, taking into account a wide range of cross-sectional slenderness and the size of the circular holes. Ban and Mei [17] studied local buckling behavior of built-up square hollow columns made of stainless-clad bimetallic steel. This study is based on the nonlinear finite element (FE) analysis and experimental tests investigation. The parametric analysis includes use of seven hollow column specimens with nominal thicknesses of 8 mm and 13 mm. The effective width methods and slenderness limitations provided by existing standards have been examined and they are concluded that the effective width techniques can often be inadequate and so from the parametric study a new design formula was proposed for the design of for SC bimetallic steel hollow columns. Liu et al. [18] presented a numerical investigation and design for the local buckling behavior of the hexagonal hollow steel columns made from the high strength steel under axial compression loads. They concluded that the Continuous Strength Method (CSM) provides forecasts that are more accurate than the Direct Strength Method (DSM). Arrayago et al. [19] studied the design of stainless steel hollow columns by using the Continuous Strength Method (CSM). They concluded that the approach (CSM) offers a framework that may be expanded to include other cross-sectional kinds and loading conditions.

The mechanical performance of the hollow steel columns is significantly impacted by sectional residual stress. The sectional residual stress have been conducted by Ban et al. [20] and Cao et al. [21]. These investigations were carried out to study the effect of the residual stress on the behavior and ultimate capacity of hollow steel columns. They concluded that the sectional residual stress has a significant effect on the buckling capacity and behavior of hollow columns under axial compression loads. Jaamala et al. [22] studied the finite element (FE) analysis of cold-formed rectangular hollow columns (CFHSC) based on a new proposed model for residual stress distributions. The proposed model is based on experimental results in this study and valid for CFRHC made of steel grades up to S960. In case of the stiffened hollow steel columns, it is observed that there

has been just a limited amount of studies conducted under monotonic loading including the local and global buckling effects. The present study aims to investigate the performance and ultimate capacity of stiffened square hollow short and long columns, under axial compression loads. Based on the non-linear finite element (FE) analysis, this investigation was carried out to evaluate the influence of major steel tube columns parameters such as stiffener length, the ratio B/t , and yield strength on the hollow steel short column's performance. The main objective of the parametric study was to develop a novel mathematical equation to predict the ultimate capacity of box steel sections. In addition, the study was conducted on effect of the stiffeners length and propose a novel equation to calculate the optimal stiffeners length. A comparison between the current (FE) results and analytical methods is presented. In case of the long columns, a comparison was made on the stiffened and unstiffened sections to investigate how the stiffeners affect the columns ultimate capacity. The numerical study is briefly described, with the variable parameters being KL_e/r and the ratio (B/t) equals to (50-12.5).

2 FINITE ELEMENT MODELING

2.1 General Description

In this investigation, the finite element software ABAQUS [35] is used to create an accurate finite element model for investigating the behavior and ultimate capacity of the steel tube columns under axial compression loads.

2.2 Initial Imperfection

The initial imperfection of the hollow square columns was considered in the load-deflection analysis. It is assumed that the first buckling mode shape obtained from the eigenvalue buckling analysis is the shape of the local and global initial imperfections. The Japan Standard for Highway Bridges (JSHB) [23] prescribes maximum initial global displacement as $(L/1000)$. The AISC 360-05 [24] prescribes maximum initial displacement as $(L/1500)$. According to experimental measurements in [13], the global imperfection in the Y- and X-directions for hollow long columns appeared to be around $(H/1200-H/1040-H/1600)$. For square hollow columns in this study, the initial imperfection value was taken as $(0.01B)$ for local buckling and $(0.001L)$ for global buckling according to Chinese Standard GB50018-2002 [25].

2.3 Residual Stresses

In the present study, according to the experimental test result by Somodi and Kövesdi [4], to estimate the compressive residual stresses, two models of the residual stress were developed. Equations (1) and (2) were developed to provide the best approximation to the

average compressive residual stresses that were measured. The “predefined field” for the initial stress option is available in FE software to model residual stress. The typical residual stress distribution of the steel square hollow stiffened and unstiffened sections are shown in Figure 1. Where σ_{rc} (MPa)

If $t \leq 5$ mm:

$$\sigma_{rc} = 70 - 2t + t^2 - (20900 - 3600t) \left(\frac{b}{t}\right)^{-1} \quad (1)$$

If $t \geq 5$ mm:

$$\sigma_{rc} = 70 - 2t + t^2 - (4350 - 290t) \left(\frac{b}{t}\right)^{-1} \quad (2)$$

Where t (mm) and b (mm) are the thickness and width of the steel box columns, respectively.

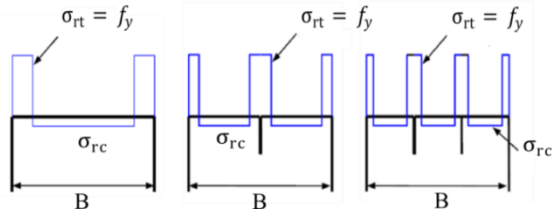


Figure 1: Residual stress distributions

2.4 Material Model

In this research, the hollow square columns material was modeled by the elastic-plastic model, as shown in Figure 2. The Poisson's ratio was considered 0.3. In addition, the plastic zone is with a linear hardening and the hardening modulus was considered $0.005E_s$ with E_s is the elastic modulus of steel [26].

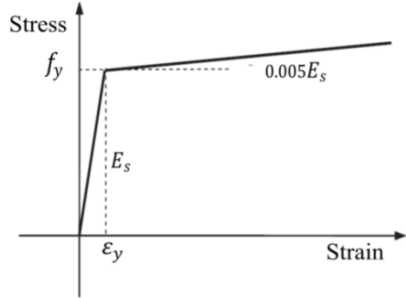


Figure 2: The stress-strain curve for steel tubes

3 FINITE ELEMENT MODELING VALIDATION

The FE model's accuracy in the present parametric study was verified using previous experimental test results. The verification study, was carried out on two short square columns that were tested by Tao et al. [2] and four long columns that were tested by Khan et al. [5].

3.1 Material and Geometric Properties

For short columns, the steel material for the finite element models was modeled as elastic-plastic model as shown in Figure 2. The yield strength $f_y = 234.3$ MPa, elastic modulus $E_s = 208$ GPa, yield strain (%) 0.137, and the ultimate strength $F_{ult} = 343.7$ MPa. The investigated specimens' labels and geometric properties are shown in Table 1 and Figure 3.

Table1. Dimensions of the stiffened and unstiffened short columns tests in Tao et al. [2]

| Specimen label | B (mm) | L (mm) | D/t | $h_s \times t_s$ |
|----------------|--------|--------|-----|------------------|
| SS25 | 250 | 750 | 100 | 35×2.5 |
| US25 | 250 | 750 | 100 | --- |

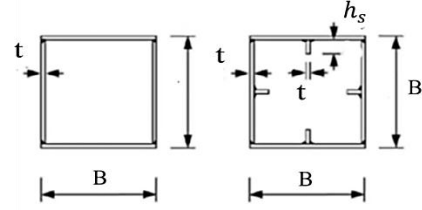


Figure 3: The specimens investigated by Tao et al. [2]

For long columns, the steel material for the finite element models was assumed to be an elastic-plastic model as shown in Figure 2. The yield strength $f_y = 762$ MPa, The elastic modulus $E_s = 213$ GPa, The yield strain 0.4157 (%), and the ultimate strength $F_{ult} = 819$ MPa. The verification was performed for slender welded box sections with $L_e/r = (77, 66, 28, \text{ and } 59)$ and $b_e/b = (1.0 \text{ and } 0.8)$. The dimensions of test specimens are shown in Table 2 and the illustration of the experimental test layout is shown in Figure 4.

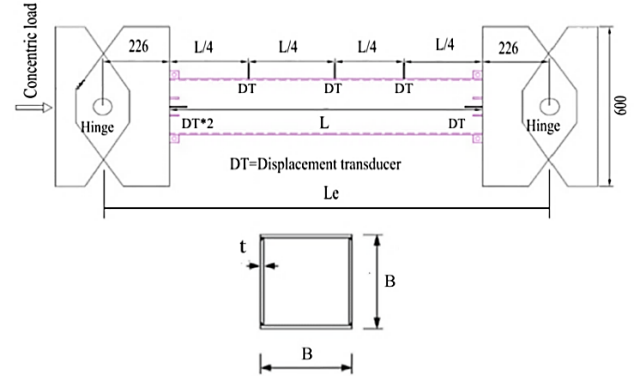


Figure 4: Illustration of the experimental test layout investigated by Khan et al. [5]

Table2. Dimensions of the test specimens for the long columns tested by Khan et al. [5]

| Test specimens | B (mm) | t (mm) | B/t | L_e (mm) | L_e/r | b_e/B |
|----------------|--------|--------|-----|------------|---------|---------|
| HS15SL2 | 74.57 | 4.93 | 15 | 2512 | 77 | 1.0 |
| HS25SL3 | 125.20 | 4.92 | 25 | 3512 | 66 | 0.8 |
| HS25SL1 | 125.21 | 4.92 | 25 | 1512 | 28 | 0.8 |
| HS20SL2 | 99.39 | 4.92 | 20 | 2512 | 59 | 1.0 |

Where:-

- b_e : The effective width.
- B : The columns width.
- r : The radius of gyration.
- L_e/r : The slenderness ratio.

3.2 Loading and Boundary Conditions

In fact, in the nonlinear analysis there are two types of loading application methods: force-controlled loading and displacement-controlled loading. In the present study, the force-controlled loading technique was used. The forced-controlled loading technique has been used in many previous researches such as [16], [27] and other researches. It gives good results especially to trace the maximum load versus displacement. In this study the (Static Riks) method was used. In nonlinear analysis, the total load applied to a finite element model is divided into a series of load increments called load steps. At the completion of each incremental solution, the stiffness matrix of the model is adjusted to reflect nonlinear changes in structural stiffness before proceeding to the next load increment. In current study the minimum limit for the increment size was also chosen to be small enough to improve the stability of the analyses. ABAQUS program uses the Arc length method for updating the model stiffness. The radius of the load factor is based on the ratio of the first buckling load. In the case of geometrically non-linear buckling analysis, ABAQUS provides the option to allow large deformation (NLGEOM), to create automatic or manual load stepping (*STEP), and arc-length step control.

The square hollow columns were modeled using the Finite Element Analysis (FEA) under monotonic loading. In case of short columns, two loading plates coupled with a steel tube by tie constraints were used. The boundary condition of the finite element (FE) model was set at the loading plate, as shown in Figure 5. The axial load was applied by carrying out a distributed load on the loading plate.

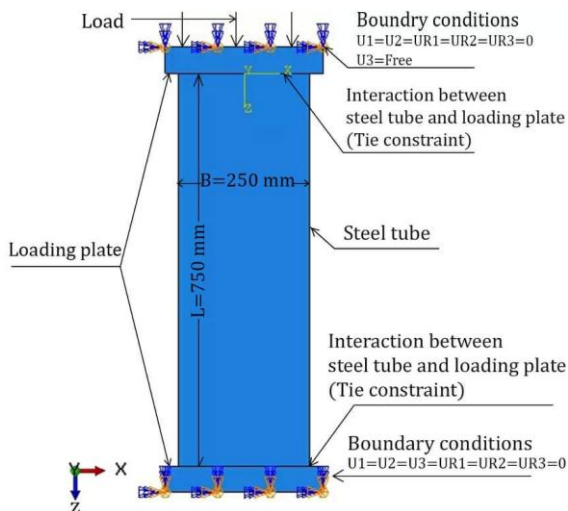


Figure 5: FE Modeling of the short columns

In the case of long columns, two reference points have been created and constrained to the loading plate of all hollow square columns specimens by rigid body constraints and set the boundary condition of the (FE) model at the reference point. Both column ends were modeled as pinned condition, i.e., both ends were free to rotate. While the upper end was unconstrained in the vertical direction to apply the external load. The square steel tube coupled with the loading plate by tie constraint is shown in Figure 6. The axial load was applied in the form of distributed load on the loading plate.

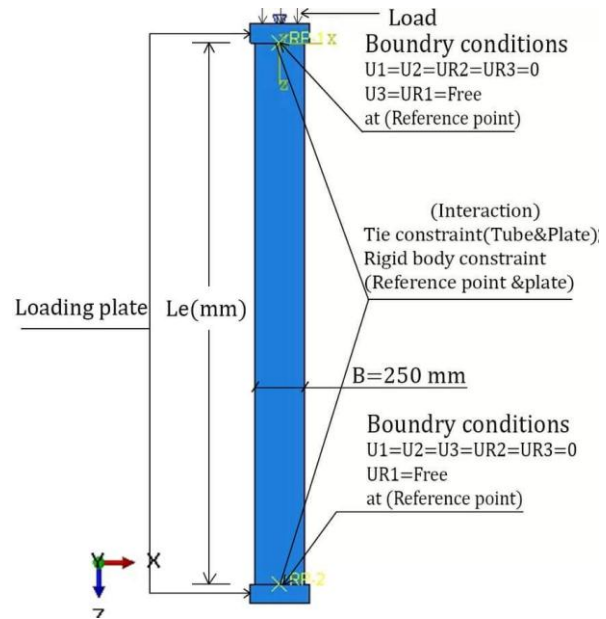


Figure 6: FE Modeling of the long columns

3.3 Element Type and Mesh

The short hollow columns in this study were modeled using 4-node reduced integration doubly curved thin or thick shell element (S4R). The loading plate was modeled using 4-node linear tetrahedron element. While in case of hollow steel long columns, the (C3D4) 4-node linear tetrahedron element was used. In addition, the approximate global element size is equal to 12 mm was used in this study based on a mesh sensitivity analysis discussed in the next section.

3.4 Accuracy of Adopted Models

3.4.1 Short Columns

The comparison of the experimental test results and the finite element results for the US25 and SS25 specimens are shown in Figure 7 and Figure 8, respectively. The mean values of the ratio between axial load deduced by FE and test (N_{FEM}/N_{Test}) are 1.02, and 1.01 for the US25 and SS25 specimens, respectively. During the verification study, a mesh sensitivity study was conducted with different mesh densities to determine the appropriate mesh density, required for the

FEA which can provide considerably accurate results. Three cases have been studied to determine effect of the mesh size on the hollow steel tube columns. The first case is a fine mesh with an approximate global size equal to 12 mm. The second case is intermediate mesh with an approximate global size equal to 20 mm. The third case is coarse mesh with an approximate global size equal to 30 mm. The comparison between the experimental test curve and the FE model at fine, intermediate, and coarse mesh shows in Figure 7 and Figure 8, respectively. From this comparison, Fig. 7 and Fig. 8, it could be seen that up to the ultimate load the results accuracy was not affected by the mesh size. While, in the post-buckling stage when the mesh size is small, the detected behavior accuracy is considerably near to the experimental test. However, there is a slight deviation in the post buckling stage which increases as the mesh size increases. In this study, the first linear buckling mode shape is used to implement the default imperfection. The effect of buckling modes on the axial load versus displacement was studied as shown in Figure 9. The buckling modes for the (US25) specimen are shown in Figure 10. From this study, the axial load versus displacement in case of the fourth buckling mode are very close to the test given by Tao et al. [2]. In addition, three initial imperfections values (0.01B, 0.002B, and 0.004B) were studied for unstiffened hollow columns to determine effect of the initial imperfections in case of the fourth buckling mode. The effect of initial imperfection for the US25 specimen shows in Figure 11. From these results it is found that the best value of the imperfection for hollow columns is 0.01B. The failure mode due to buckling obtained from the geometric nonlinear buckling FE analysis is shown in Figure 12.

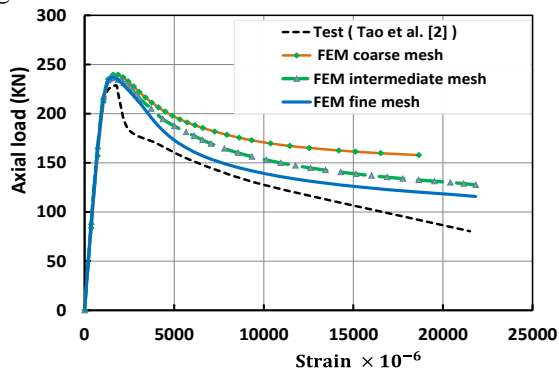


Figure 7: Comparison of the experimental test results (by Tao et al. [2]) and the current finite element results for the (US25) specimen

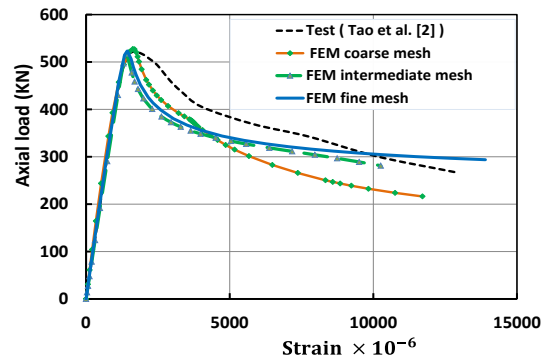


Figure 8: Comparison of the experimental test results (by Tao et al. [2]) and the current finite element results for the (SS25) specimen

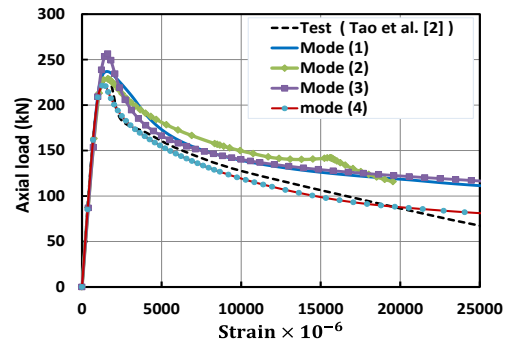
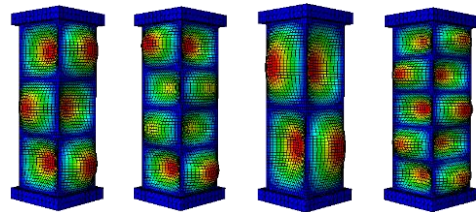


Figure 9: Effect of the buckling mode for the (US25) specimen



Mode (1) Mode (2) Mode (3) Mode (4)
Figure 10: The buckling modes from linear buckling analysis for the (US25) specimen

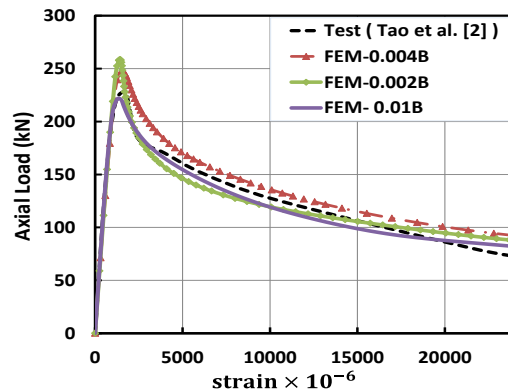


Figure 11: Effect of the initial geometrical imperfections for the (US25) Specimen

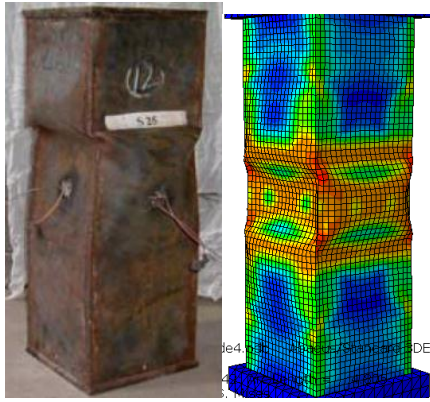


Figure 12: Comparison between the local buckling failure modes of the test (Tao et al. [2]) and the current FE model for the (US25) specimen

3.4.2 Long Columns

Comparisons between the experimental test results and the finite element (FE) results for the HS15SL2, HS25SL3, HS25SL1, and HS20SL2 specimens are shown in Figure 13, Figure 14, Figure 15, and Figure 16, respectively. The mean values of N_{FEM}/N_{Test} are, respectively, 1.01, 1.03, 1.02, and 0.99 for the HS15SL2, HS25SL3, HS25SL1, and HS20SL2 specimens. The initial global imperfections have a significant effect on the behavior of hollow steel columns, and therefore it has been studied. Three initial imperfections values were studied for the hollow long columns to determine effect of the initial imperfections on ultimate capacity. The three values used are $L_e/1000$, $L_e/1200$, and $L_e/1500$. The effect of initial imperfection on the (HS15SL2) and the (HS25SL3) specimens is shown in Figure 13 and Figure 14, respectively. From this study the value of $L_e/1000$ in amplitudes of the initial global imperfections for hollow steel columns gives the best results. The predicted ultimate capacity are very close to the given by tests in Khan et al. [5]. However, there is a slight deviation in the post buckling stage. For the long columns, the mesh sensitivity study was conducted with two different mesh sizes to determine the appropriate mesh density, required for the FEA which can provide considerably accurate results. Two cases have been studied to determine effect of the mesh size on the hollow steel long columns. The first case is a fine mesh with an approximate global size equal to 12 mm. The second case is coarse mesh with an approximate global size equal to 16 mm. The comparison between the experimental test curve and the FE model at fine and coarse mesh for the HS25SL1 and the HS20SL2 specimens are shows in Figure 15 and Figure 16, respectively. The fine mesh with an approximate global size equal to 12 mm can provide relatively good results especially to predict the ultimate load. As a result, it was used in the current study. The HS15SL2 and HS20SL2 specimens with unstiffened compact section with $b_e/b = 1$ and $L_e/r = 77$ and 59, respectively, failed due

to global buckling only. The comparison of the buckling modes for the experimental test and FE model is shown in Figure 17 for the HS15SL2 specimen. The HS25SL3 and HS25SL1 specimens, with unstiffened slender sections with $b_e/b = 0.8$ and $L_e/r = 66$ and 28, respectively, failed due to interaction between global and local buckling. The failure buckling modes for the HS25SL3 and HS25SL1 specimens are shown in Figure 18.

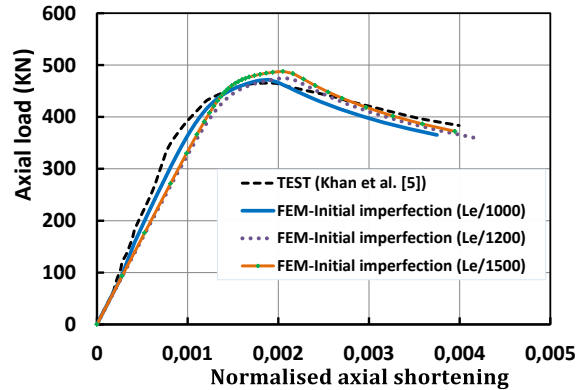


Figure 13: Comparison of the experimental test results (Khan et al. [5]) and the finite element results for the HS15SL2 specimen

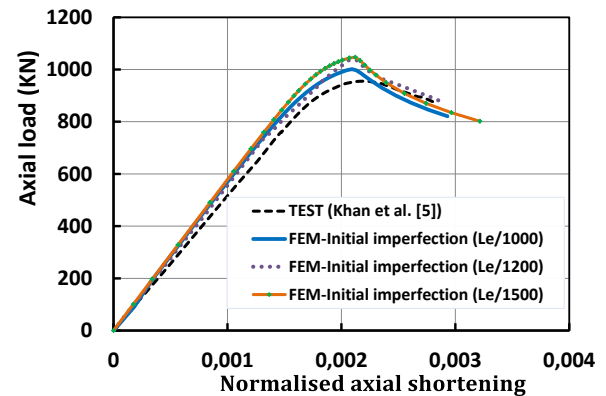


Figure 14: Comparison of the experimental test results (Khan et al. [5]) and the finite element results for the HS25SL3 specimen

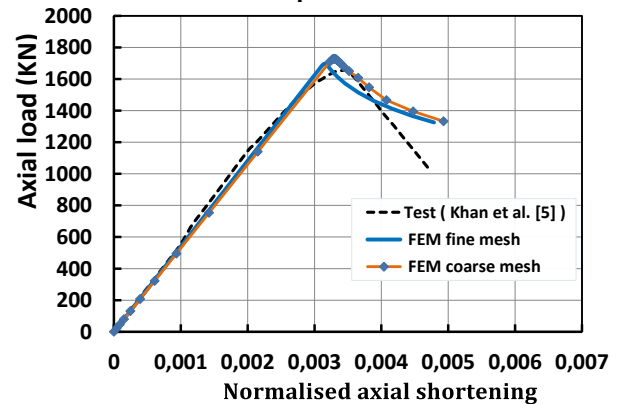


Figure 15: Comparison of the experimental test results (Khan et al. [5]) and the finite element results for the HS25SL1 specimen

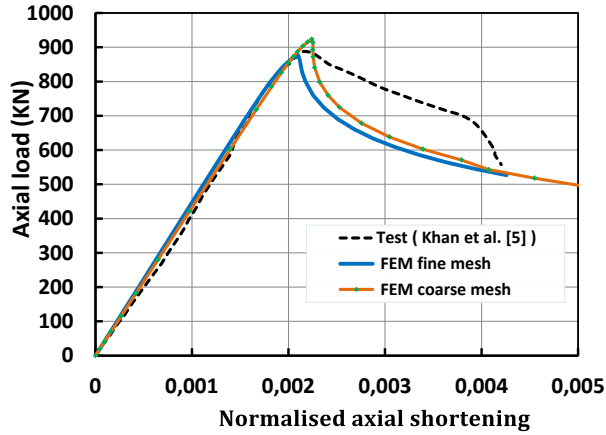


Figure 16: Comparison of the experimental test results (Khan et al. [5]) and the finite element results for the HS20SL2 specimen

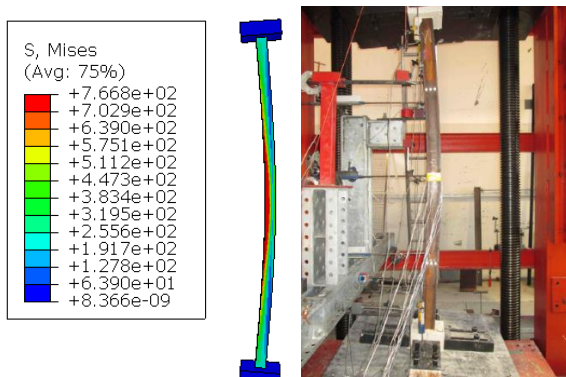


Figure 17: Comparison of the buckling mode for the experimental test (Khan et al. [5]) and FE model for the HS15SL2 specimen

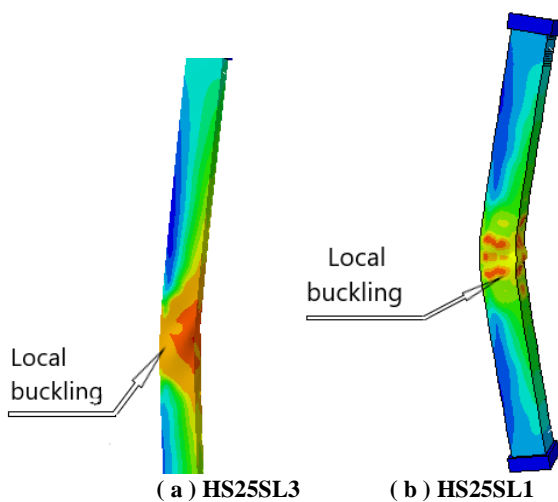


Figure 18: The long column global and local buckling modes for the unstiffened tube column

4 PARAMETRIC STUDY

4.1 General Description

Based on the verification study a parametric investigation was carried out to create three-dimensional finite element models that simulate the stiffened and unstiffened hollow steel columns under axial compression. These models focused on the global and local buckling and were divided into two cases. The first one investigated the effect of local buckling on the behavior and ultimate capacity of short steel hollow columns. The second case investigated the influence of stiffeners on the ultimate capacity and performance of long steel hollow columns. The non-linear finite element (FE) analysis is used in the study to understand the effect of main structural parameters such as L_e/r , stiffener length, the ratio of width-to-thickness B/t , and the yield stress on the hollow steel column performance.

4.2 Columns Geometry

4.2.1 Short Columns

The steel material model for the finite elements was assumed to be an elastic-plastic model as shown in Figure 2, taken a hardening coefficient equal to $0.005E_s$. The Young's modulus $E_s = 200000$ MPa and Poisson's ratio $\nu = 0.3$. The studied parameters were the yield strength $f_y = 240, 360, 460, 560,$ and 779 MPa, the stiffeners length (h_s), and the ratio B/t . The columns length is $L = 750$ mm and the column width is $B = 250$ mm for all the specimens. The thickness of the stiffeners is considered equal to the thickness of the tube, as listed in Tables (3 and 4). The shapes and dimensions of the investigated steel columns are shown in Figure 19. The specimen label shows whether the sections is unstiffened (US), stiffened using single stiffener per section wall (SS), or stiffened using double stiffener per section wall (DS). In addition, the label suffixed by the thickness of the section walls in (mm).

The boundary condition as described previously and shown in Figure 5. For square hollow columns, the initial local imperfection value has been set to $0.01B$. In addition, this study used the distribution of residual stress shown in Figure 1. The columns in this study were modeled using 4-node shell elements (S4R) and the approximate global size of the mesh is about 12 mm.

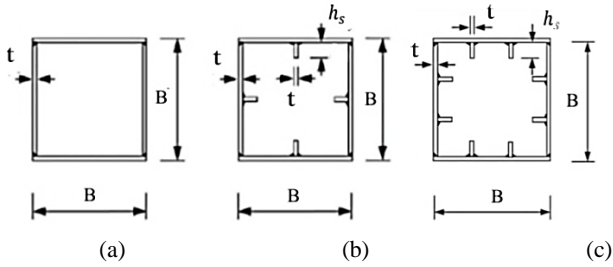


Figure 19: The investigated cross-sections' shapes and dimensions; (a) Unstiffened sections US, (b) Stiffened sections with one stiffener SS, (c) Stiffened sections with two stiffeners DS

Table3. The parameters and dimensions of hollow steel short columns used in the parametric study

| Unstiffened sections (US) | | | Stiffened sections with one stiffener (SS) | | | Stiffened sections with two stiffeners (DS) | | |
|---------------------------|--------------|---------------|--------------------------------------------|--------------|---------------|---------------------------------------------|--------------|---------------|
| t mm | f_y MPa | $\frac{B}{t}$ | t mm | f_y MPa | $\frac{B}{t}$ | t mm | f_y MPa | $\frac{B}{t}$ |
| 1 | 240 | 250 | 1 | 240 | 250 | 1 | 240 | 250 |
| 1.5 | 240 | 167 | 2 | 240 | 125 | 2.5 | 240 | 100 |
| 2 | 240 | 125 | 2.8 | 240 | 89 | 4 | 240 | 63 |
| 3.2 | 240 | 78 | 4.5 | 240 | 55 | 6 | 240 | 42 |
| 5.1 | 240 | 48 | 6.7 | 240 | 37 | 8 | 240 | 31 |
| 7.7 | 240 | 32 | 9 | 240 | 28 | 1 | 360 | 250 |
| 10 | 240 | 25 | 1 | 360 | 250 | 2.5 | 360 | 100 |
| 16 | 240 | 16 | 2 | 360 | 125 | 4 | 360 | 63 |
| 1 | 360 | 250 | 2.8 | 360 | 89 | 6 | 360 | 42 |
| 1.5 | 360 | 167 | 4.5 | 360 | 55 | 8 | 360 | 31 |
| 2 | 360 | 125 | 6.7 | 360 | 37 | 1 | 460 | 250 |
| 3.2 | 360 | 78 | 9 | 360 | 28 | 2.5 | 460 | 100 |
| 5.1 | 360 | 48 | 1 | 460 | 250 | 4 | 460 | 63 |
| 7.7 | 360 | 32 | 2 | 460 | 125 | 6 | 460 | 42 |
| 10 | 360 | 25 | 2.8 | 460 | 89 | 8 | 460 | 31 |
| 16 | 360 | 16 | 4.5 | 460 | 55 | 1 | 560 | 250 |
| 1 | 460 | 250 | 6.7 | 460 | 37 | 2.5 | 560 | 100 |
| 1.5 | 460 | 167 | 9 | 460 | 28 | 4 | 560 | 63 |
| 2 | 460 | 125 | 1 | 560 | 250 | 6 | 560 | 42 |
| 3.2 | 460 | 78 | 2 | 560 | 125 | 8 | 560 | 31 |
| 5.1 | 460 | 48 | 2.8 | 560 | 89 | 1 | 779 | 250 |
| 7.7 | 460 | 32 | 4.5 | 560 | 55 | 2.5 | 779 | 100 |
| 10 | 460 | 25 | 6.7 | 560 | 37 | 4 | 779 | 63 |
| 16 | 460 | 16 | 9 | 560 | 28 | 6 | 779 | 42 |
| 1 | 560 | 250 | 1 | 779 | 250 | 8 | 779 | 31 |
| 1.5 | 560 | 167 | 2 | 779 | 125 | - | - | - |
| 2 | 560 | 125 | 2.8 | 779 | 89 | - | - | - |
| 3.2 | 560 | 78 | 4.5 | 779 | 55 | - | - | - |
| 5.1 | 560 | 48 | 6.7 | 779 | 37 | - | - | - |
| 7.7 | 560 | 32 | 9 | 779 | 28 | - | - | - |
| 10 | 560 | 25 | 11.3 | 779 | 22.1 | - | - | - |
| 16 | 560 | 16 | 12 | 779 | 20.8 | - | - | - |
| Unstiffened sections (US) | | | | | | | | |
| 1 | 779 | 250 | 7.7 | 779 | 32 | 1 | 779 | 250 |
| 1.5 | 779 | 167 | 10 | 779 | 25 | 1.5 | 779 | 167 |
| 2 | 779 | 125 | 16 | 779 | 16 | 2 | 779 | 125 |
| 3.2 | 779 | 78 | 18 | 779 | 13.8 | 3.2 | 779 | 78 |
| 5.1 | 779 | 48 | 20 | 779 | 12.5 | 5.1 | 779 | 48 |

Table4. The stiffeners length (h_s) of stiffened hollow steel short columns used in the parametric study, where $f_y = 779 \text{ MPa}$

| Stiffened sections with one stiffener (SS) | | Stiffened sections with one stiffener (SS) | | Stiffened sections with two stiffeners (DS) | | Stiffened sections with two stiffeners (DS) | |
|--------------------------------------------|-------------|--------------------------------------------|-------------|---------------------------------------------|-------------|---------------------------------------------|-------------|
| t mm | h_s mm | t mm | h_s mm | t mm | h_s mm | t mm | h_s mm |
| 1 | 10 | 1 | 40 | 2 | 10 | 2 | 50 |
| 1.5 | 10 | 1.5 | 40 | 3.2 | 10 | 3.2 | 50 |
| 2 | 10 | 2 | 40 | 5.1 | 10 | 5.1 | 50 |
| 3.2 | 10 | 3.2 | 40 | 7.7 | 10 | 7.7 | 50 |
| 5.1 | 10 | 5.1 | 40 | 10 | 10 | 10 | 50 |
| 7.7 | 10 | 7.7 | 40 | 16 | 10 | 16 | 50 |
| 10 | 10 | 10 | 40 | 2 | 20 | 2 | 60 |
| 16 | 10 | 16 | 40 | 3.2 | 20 | 3.2 | 60 |
| 1 | 20 | 1 | 50 | 5.1 | 20 | 5.1 | 60 |
| 1.5 | 20 | 1.5 | 50 | 7.7 | 20 | 7.7 | 60 |
| 2 | 20 | 2 | 50 | 10 | 20 | 10 | 60 |
| 3.2 | 20 | 3.2 | 50 | 16 | 20 | 16 | 60 |
| 5.1 | 20 | 5.1 | 50 | 2 | 30 | - | - |
| 7.7 | 20 | 7.7 | 50 | 3.2 | 30 | - | - |
| 10 | 20 | 10 | 50 | 5.1 | 30 | - | - |
| 16 | 20 | 16 | 50 | 7.7 | 30 | - | - |
| 1 | 30 | 1 | 60 | 10 | 30 | - | - |
| 1.5 | 30 | 1.5 | 60 | 16 | 30 | - | - |
| 2 | 30 | 2 | 60 | 2 | 40 | - | - |
| 3.2 | 30 | 3.2 | 60 | 3.2 | 40 | - | - |
| 5.1 | 30 | 5.1 | 60 | 5.1 | 40 | - | - |
| 7.7 | 30 | 7.7 | 60 | 7.7 | 40 | - | - |
| 10 | 30 | 10 | 60 | 10 | 40 | - | - |
| 16 | 30 | 16 | 60 | 16 | 40 | - | - |

4.2.2 Long Columns

The steel material for the finite element models was assumed to be an elastic-plastic with linear hardening model. Moreover, the hardening modulus has been set to equal to $0.005E_s$ as shown in Figure 2. The Young's modulus $E_s = 200000 \text{ MPa}$ and the Poisson's ratio $\nu = 0.3$. The boundary condition as described previously and shown in Figure 6. For square hollow columns, the initial global imperfection value was taken as $0.001L$. The studied parameters were the columns length (L) and the ratio (B/t), as listed in Tables (5 and 6). In addition, the columns width $B = 250 \text{ mm}$ for all specimens, the yield strength is used in this study $f_y = 779 \text{ MPa}$, and the stiffeners length $h_s = 35 \text{ mm}$. The thickness of the stiffener is the same as the thickness of the tube. The specimens investigated are shown in Figure 20. The specimens' labels are as follows:

- (US - t - L) = (US) Unstiffened section - (t) thickness - (L) column length.
- (SS - t - L) = (SS) Stiffened section with one stiffener-(t) thickness - (L) column length.

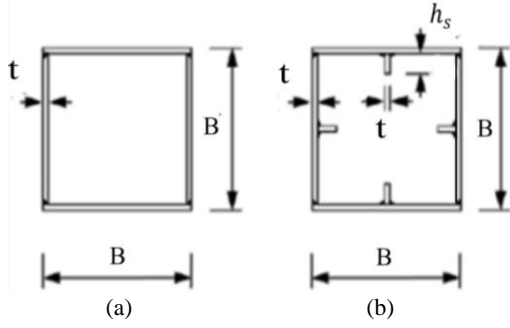


Figure 20: The cross-sections investigated in the current study and the manufacturing method; (a) Unstiffened section, (b) Stiffened section with one stiffener per wall.

Table 5. The dimensions of the unstiffened section, where the ratio $(B/t) = 12.5$ and 50

| No. | Specimen label | (B/t) | $\frac{KL_e}{r}$ |
|-----|----------------|---------|------------------|
| 1 | US-20-2750 | 12.5 | 29.2 |
| 2 | US-20-3000 | 12.5 | 31.8 |
| 3 | US-20-4000 | 12.5 | 42.4 |
| 4 | US-20-5000 | 12.5 | 53 |
| 5 | US-20-6000 | 12.5 | 63.7 |
| 6 | US-20-7000 | 12.5 | 74.3 |
| 7 | US-20-8000 | 12.5 | 84.9 |
| 8 | US-5-3000 | 50 | 30 |
| 9 | US-5-4000 | 50 | 40 |
| 10 | US-5-5000 | 50 | 50 |
| 11 | US-5-6000 | 50 | 60 |
| 12 | US-5-7000 | 50 | 70 |
| 13 | US-5-8000 | 50 | 80 |
| 14 | US-5-9000 | 50 | 90 |

Table 6. The dimensions of the stiffened sections with one stiffener, where the ratio $(B/t) = 12.5$ and 50

| No. | Specimen label | (B/t) | $\frac{KL_e}{r}$ |
|-----|----------------|---------|------------------|
| 1 | SS-20-3000 | 12.5 | 33.1 |
| 2 | SS-20-4000 | 12.5 | 44.1 |
| 3 | SS-20-5000 | 12.5 | 55.1 |
| 4 | SS-20-6000 | 12.5 | 66.2 |
| 5 | SS-20-7000 | 12.5 | 77.2 |
| 6 | SS-20-8000 | 12.5 | 88.2 |
| 7 | SS-20-9000 | 12.5 | 99.2 |
| 8 | SS-5-1000 | 50 | 10.3 |
| 9 | SS-5-2000 | 50 | 20.6 |
| 10 | SS-5-3000 | 50 | 30.9 |
| 11 | SS-5-4000 | 50 | 41.2 |
| 12 | SS-5-5000 | 50 | 51.5 |
| 13 | SS-5-6000 | 50 | 61.8 |
| 14 | SS-5-7000 | 50 | 72.1 |
| 15 | SS-5-8000 | 50 | 82.4 |

4.3 Results and Discussion of the Parametric Study

4.3.1 Unstiffened Short Columns FE Results Against Analytical Methods

Most standards and specifications use the effective width approach to consider the local buckling in case of the slender hollow steel tube cross-sections. This theory was developed based on redistribution of the stress on a steel tube with the average ultimate stress σ_u as shown in Figure 21. According to Von Karman et al. [32], the effective width b_e is the only part of the width that can resist the loading, but there is no loading on the plate central part. The effective width is represented in Figure 21(b).

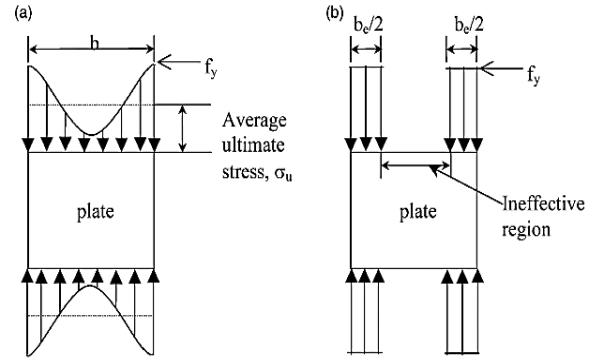


Figure 21: (a) Distribution of ultimate stress, (b) Concept of effective width in a compressed plate according to Von Karman et al. [32]

The values of σ_{ult}/f_y in Table 7 give the reduction factors of the strength for the numerical models, where $\sigma_{ult} = N_s/A_s$. Where, N_s represents the ultimate loads, takes into account the reduction due to local buckling effects according to the effective width approach by Uy [28]. The local buckling reduction factor (b_e/b) is determined using Eq. (3) and (4), where the ratio (b_e/b) is the effective tube width ratio to full tube width. When (b_e/b) equals 1.0, this means that the sections are compact.

$$\frac{b_e}{b} = \alpha \sqrt{\frac{\sigma_{ol}}{\sigma_y}} \quad (3)$$

Where $\alpha = 0.651$ for heavily welded tubes. Which accounts for geometric imperfections and residual stress. The stress of local buckling σ_{ol} is presents in Eq. (4), as shown below:

$$\sigma_{ol} = \frac{K\pi^2 E_s}{12(1 - \nu^2)(b/t)^2} \quad (4)$$

Where the coefficient of plate buckling (K) can be considered as 4 for hollow sections and $N_s = (b_e/b)A_s f_y$. Von Karman et al. [32] developed the first effective width expression in 1932. This expression states that a width of plate (b) and effective width (b_e)

can be used to evaluate the ultimate strength capacity. Von Karman's effective width can be written in terms of the yield stress σ_y and critical stress σ_{CR} as follows:

$$\frac{b_e}{b} = \sqrt{\frac{\sigma_{CR}}{\sigma_Y}} \quad (5)$$

Where:

$$\sigma_{CR} = \frac{K\pi^2 E t^2}{12(1-\nu^2)b^2} \quad (6)$$

Where the buckling coefficient $K = 4$ in case of the simply supported plate. Winter [33] subsequently modified von Karman's equation to:

$$\frac{b_e}{b} = \sqrt{\frac{\sigma_{CR}}{\sigma_E}} \left(1 - 0.25 \sqrt{\frac{\sigma_{CR}}{\sigma_E}} \right) \quad (7)$$

The second term within the bracket out Winter equation is mainly at the point where the applied edge stress σ_E and yield stress σ_y are similar. According to the Direct Strength Method (DSM) by ANSI/AISI S100-16 [29], the theoretical equation to estimate the ultimate loads accounting for the local buckling as given in Eq. (8). Where the $P_{cr,T}$ is the critical elastic local buckling load of the square hollow columns and λ_l is the non-dimensional cross-section slenderness of the cross-section and equals to $\lambda_l = (f_y A_g / P_{cr,T})^{0.5}$.

$$N_{DSM} = \begin{cases} f_y \times A_g, & \text{for } \lambda_l \leq 0.776 \\ \left(1 - \frac{0.15}{\lambda_l^{0.8}} \right) \frac{1}{\lambda_l^{0.8}} f_y \times A_g, & \text{for } \lambda_l > 0.776 \end{cases} \quad (8)$$

Where f_y in (MPa) and A_g in (mm^2).

Fang and Chan [30] modified the direct strength method to give the predictions of safer strength for welded steel hollow columns, as shown in Eq. (9).

$$N_{DSM}^{\#} = \begin{cases} f_y \times A_g, & \text{for } \lambda_l \leq 0.707 \\ \left(\frac{0.96}{\lambda_l^{0.9}} - \frac{0.22}{\lambda_l} \right) f_y \times A_g, & \text{for } \lambda_l > 0.707 \end{cases} \quad (9)$$

In this investigation, the main objective of the analytical methods is to study the local buckling effect on the steel tube ultimate capacity and compare with the current (FE) results. Eight FE models of unstiffened short columns was studied in this case, where the (B/t) ratio varying from 16 to 250. According to most of the international codes like ANSI/AISC 360-16 [34] the dimensions used in this investigation provide valuable data for slender, non-compact, and compact sections. The hollow steel sections, according to ANSI/AISC 360-16 are classified for local buckling.

- $\lambda \leq \lambda_p$ The tube is a compact section.
- $\lambda_r \geq \lambda > \lambda_p$ The tube is a non-compact section.
- $\lambda > \lambda_r$ The tube is a slender cross-section.

Where:

$$\lambda_p = 1.12 \sqrt{E/F_y} \quad (10)$$

$$\lambda_r = 1.40 \sqrt{E/F_y} \quad (11)$$

$$\lambda = B/t \quad (12)$$

The comparison of the analytical and the FE results for the unstiffened steel columns is summarized in Figure 22 and Table (7a-7b). According to this comparison, the present FE results produces conservative predictions of the steel tube ultimate capacity. In addition, the average variation between current FE models and the effective width approach by Uy [28] is around 4%. Additionally, the average variation between current FE models and modified (DSM) is around 6%. From this comparison, the results of present (FE) and the effective width method by Uy [28] are approximately similar. This is because both the current FE models and the effective width method by Uy [28] take into account the geometric imperfections and residual stress. Thus, it can be concluded that the proposed FE models can accurately predict the ultimate load capacity of short columns.

Table7a. FE results of unstiffened sections (US) for $f_y = 779$ MPa

| Specimen label | $\frac{B}{t}$ | σ_{ult}/f_y | | |
|----------------|---------------|--------------------|---------|-------------------|
| | | Present FEM | Uy [28] | Modified DSM [30] |
| US-1 | 250 | 0.11 | 0.09 | 0.12 |
| US-1.5 | 167 | 0.16 | 0.14 | 0.17 |
| US-2 | 125 | 0.19 | 0.18 | 0.22 |
| US-3.2 | 78 | 0.29 | 0.30 | 0.33 |
| US-5.1 | 48 | 0.40 | 0.42 | 0.50 |
| US-7.7 | 32 | 0.66 | 0.63 | 0.72 |
| US-10 | 25 | 0.82 | 0.81 | 0.90 |
| US-16 | 16 | 0.96 | 1.00 | 1.00 |

Table7b. FE results of unstiffened sections (US) for $f_y = 779$ MPa

| Specimen label | $\frac{B}{t}$ | σ_{ult}/f_y | | |
|----------------|---------------|--------------------|----------|------------------|
| | | Winter [33] | DSM [29] | Von Karmans [32] |
| US-1 | 250 | 0.12 | 0.18 | 0.12 |
| US-1.5 | 167 | 0.17 | 0.25 | 0.18 |
| US-2 | 125 | 0.23 | 0.31 | 0.24 |
| US-3.2 | 78 | 0.35 | 0.44 | 0.39 |
| US-5.1 | 48 | 0.53 | 0.62 | 0.63 |
| US-7.7 | 32 | 0.72 | 0.83 | 0.95 |
| US-10 | 25 | 0.85 | 0.98 | 1.00 |
| US-16 | 16 | 1.00 | 1.00 | 1.00 |

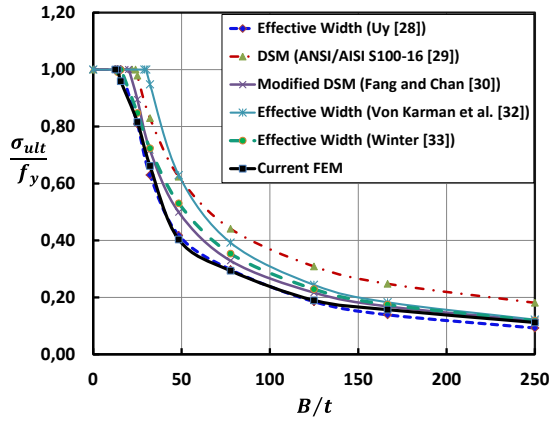


Figure 22: Comparison between the present FE results and analytical methods for unstiffened columns, where $f_y = 779 \text{ MPa}$

4.3.2 Stiffened Short Columns FE Results Against Analytical Methods

This case deals with stiffeners in steel tube subjected to axial stress. There are two primary types of stiffeners:

- Longitudinal stiffeners, that are aligned with the steel tube length direction.
- Transverse stiffeners, that are aligned normal to the length direction of the steel tube.

The stiffeners can be attached to the four walls of the tube, and it is used to control the local buckling of this tube. In this study, the steel tube is without transverse stiffeners, so it is possible that the stiffener could buckle locally or could be ineffective when the stiffener length is small. There are different formulas to account for stiffeners such as the effective plate width according to Norsok standard (N-004) [31]. This standard was developed depending on a steel tube redistribution of stress as shown in Figure 23. The effective width s_e for the stiffened sections subjected to longitudinal stress is found from:

$$\frac{s_e}{s} = C_{xs} C_{ys} C_{\tau s} \quad (13)$$

The reduction factor in the longitudinal direction, C_{xs} , is found from:

$$C_{xs} = \frac{\bar{\lambda}_p - 0.22}{\bar{\lambda}_p^2} \quad , \text{ if } \bar{\lambda}_p > 0.673 \quad (14)$$

$$C_{xs} = 1 \quad , \quad \text{ if } \bar{\lambda}_p \leq 0.673 \quad (15)$$

Where:

$$\bar{\lambda}_p = 0.525 \frac{s}{t} \sqrt{\frac{f_y}{E}} \quad (16)$$

C_{ys} is the reduction factor for compression stresses in the transverse direction.

$C_{\tau s}$ is the reduction factor for shear.

The comparison of the analytical results and the FE results is summarized in Figure 24 for the stiffened

sections with one stiffener, where $h_s = 35 \text{ mm}$ and $f_y = 779 \text{ MPa}$. The Norsok standard does not consider the effect of the stiffener length in calculating the section capacity. In this case, the stiffeners may fail due to the local buckling. Therefore, the current FE results produce conservative predictions of the steel tube ultimate capacity for stiffened steel columns. In addition, the average variation between current FE models and the effective width method by Norsok is around 6%. In this case, where $B/t \leq 70$, the prediction of ultimate capacity by current FE is very close to the effective width method by Norsok. This is because the stiffeners most likely is not exhibiting any local buckling. In addition, where $B/t > 70$ the current FE results produce conservative predictions of the ultimate capacity. This is because the stiffeners most likely is exhibiting local buckling.

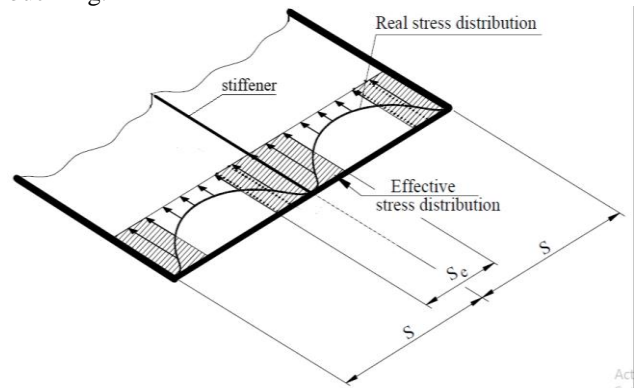


Figure 23: Effective width concept in stiffened plate under compression

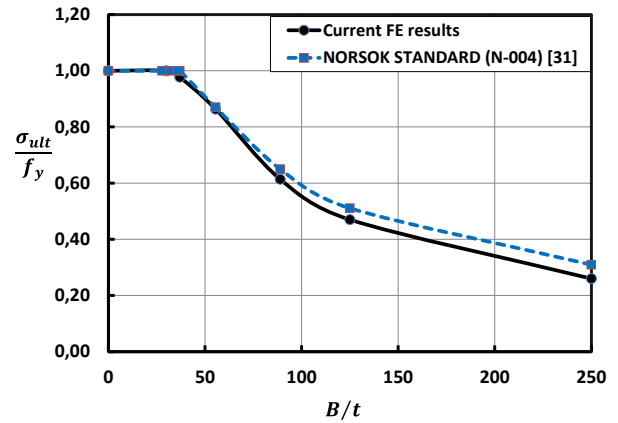


Figure 24: Comparison between the current FE results and analytical methods for the stiffened sections with one stiffener, where $h_s = 35 \text{ mm}$ and $f_y = 779 \text{ MPa}$

4.3.3 Comparison between Stiffened and Unstiffened Hollow Short Steel Columns

The proposed stiffening system may be improved by arranging the stiffeners properly, which can even change the strain softening properties. The steel tube dimensions were selected to provide relatively slender, non-compact, and compact sections. The numerical results for the unstiffened and stiffened steel hollow columns are summarized in Tables 8 and Tables 9, respectively. According to these results, the capacity of the stiffened steel tube hollow columns is remarkably higher than those of the unstiffened columns. The unstiffened and stiffened square steel tube columns primarily collapsed due to local buckling but at different modes, as shown in Figure 31 for US-4, SS-4, and DS-4 specimens, respectively. Figure 27 shows the ultimate capacity curves of the US, SS, and the DS sections. The ultimate capacity σ_{ult} are normalized by dividing by f_y . The stress distributions for the US-2.5, SS-2.5, and DS-2.5 specimens are shown in Figure 25 and Figure (26a and b), respectively. The proposed stiffening method can enhance the steel tube ultimate ductility and capacity. The collapsed modes of the steel columns indicate that the stiffening scheme effectively delays local buckling.

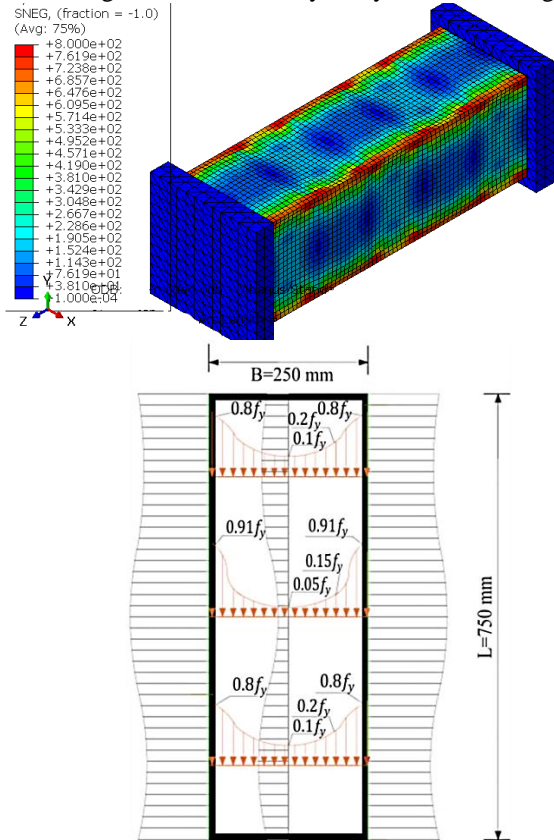
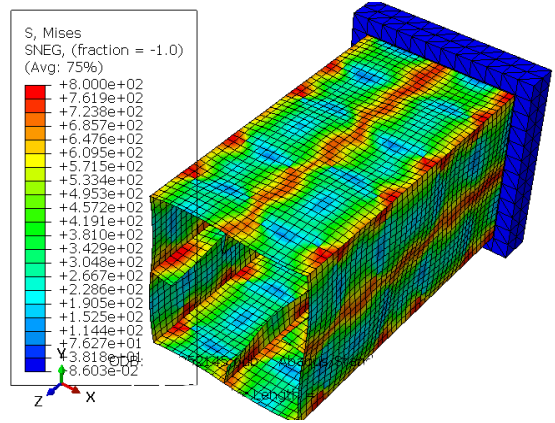
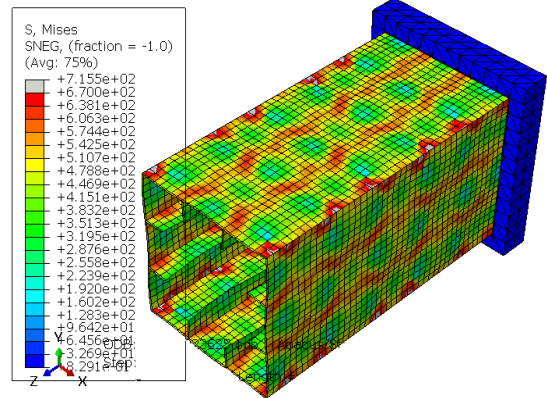


Figure 25: Stress distribution on the unstiffened columns at ultimate load for the US-2.5 specimen, where $f_y = 779 \text{ MPa}$



(a) SS-2.5 specimen



(b) DS-2.5 specimen

Figure 26: Stress distribution on the stiffened sections at ultimate load, where $f_y = 779 \text{ MPa}$ and stiffeners length $h_s = 35 \text{ mm}$.

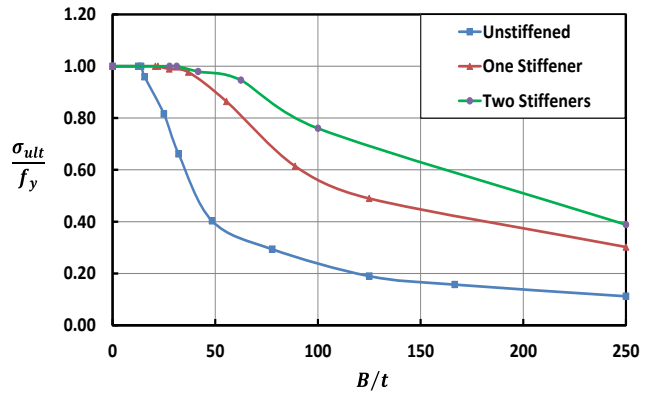


Figure 27: A Comparison between the unstiffened and stiffened steel tube columns, where $h_s = 35 \text{ mm}$ and $f_y = 779 \text{ MPa}$

Table8. FE results of the unstiffened columns

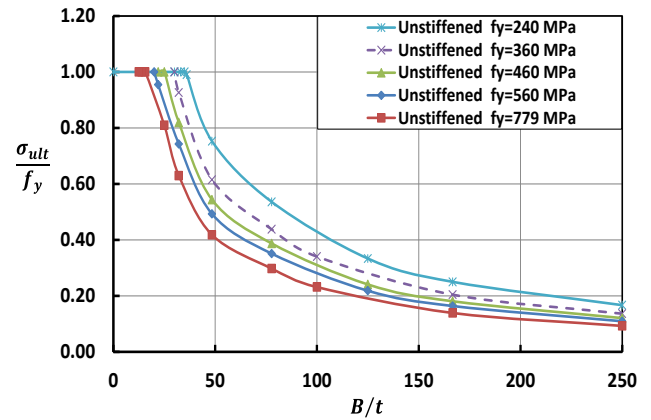
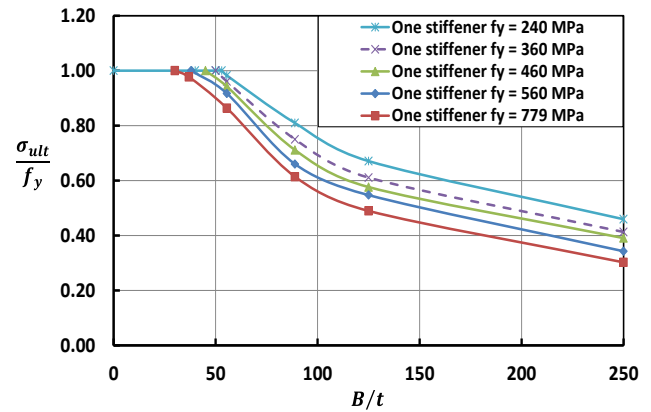
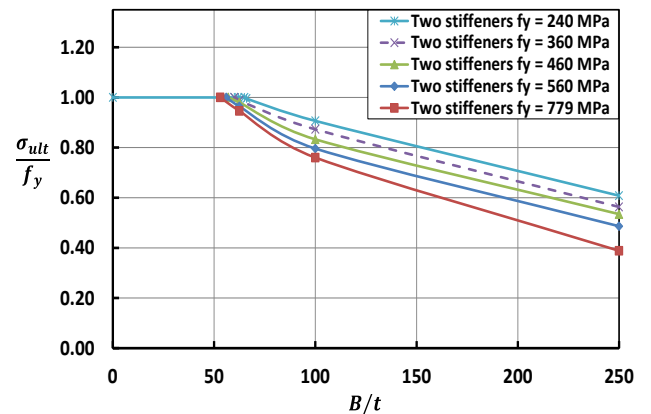
| Specimen label | $\frac{B}{t}$ | σ_{ult}/f_y at f_y (MPa) | | | | |
|----------------|---------------|-----------------------------------|---------|---------|---------|---------|
| | | 240 MPa | 360 MPa | 460 MPa | 560 MPa | 779 MPa |
| US-1 | 250 | 0.17 | 0.14 | 0.12 | 0.11 | 0.11 |
| US-1.5 | 167 | 0.25 | 0.20 | 0.18 | 0.16 | 0.16 |
| US-2 | 125 | 0.33 | 0.27 | 0.24 | 0.22 | 0.19 |
| US-3.2 | 78 | 0.54 | 0.44 | 0.39 | 0.35 | 0.29 |
| US-5.1 | 48 | 0.75 | 0.61 | 0.54 | 0.49 | 0.40 |
| US-7.7 | 32 | 0.99 | 0.93 | 0.82 | 0.74 | 0.66 |
| US-10 | 25 | 1.00 | 1.00 | 1.00 | 0.95 | 0.82 |
| US-16 | 16 | 1.00 | 1.00 | 1.00 | 1.00 | 0.96 |

Table9. FE results of the stiffened sections with one and two stiffeners, where the stiffeners length $h_s = 35$ mm

| Specimen label | $\frac{B}{t}$ | σ_{ult}/f_y at f_y (MPa) | | | | |
|----------------|---------------|-----------------------------------|---------|---------|---------|---------|
| | | 240 MPa | 360 MPa | 460 MPa | 560 MPa | 779 MPa |
| SS-1 | 250 | 0.46 | 0.41 | 0.39 | 0.34 | 0.3 |
| SS-2 | 125 | 0.67 | 0.61 | 0.58 | 0.55 | 0.49 |
| SS-2.8 | 89 | 0.81 | 0.75 | 0.71 | 0.66 | 0.61 |
| SS-4.5 | 55 | 0.98 | 0.96 | 0.94 | 0.92 | 0.86 |
| SS-6.7 | 37 | 0.99 | 0.98 | 0.96 | 0.99 | 0.98 |
| SS-9 | 28 | 1.00 | 1.00 | 1.00 | 1.00 | 1.00 |
| DS-1 | 250 | 0.61 | 0.56 | 0.53 | 0.49 | 0.39 |
| DS-2.5 | 100 | 0.91 | 0.87 | 0.83 | 0.8 | 0.76 |
| DS-4 | 63 | 1.00 | 0.99 | 0.98 | 0.96 | 0.95 |
| DS-6 | 42 | 1.00 | 1.00 | 0.99 | 0.98 | 0.98 |
| DS-8 | 31 | 1.00 | 1.00 | 1.00 | 1.00 | 1.00 |

4.3.4 Effect of Yield Strength of Hollow Short Steel Columns

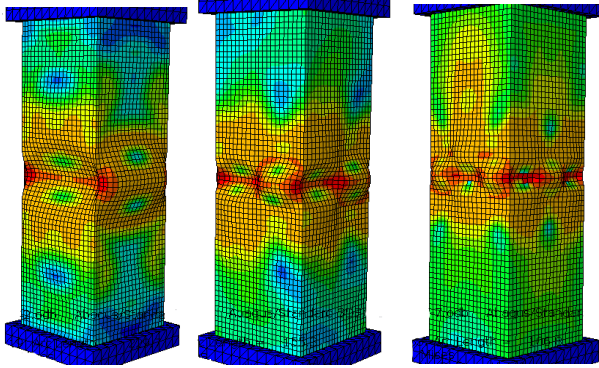
In recent years, the yield strengths of structural steel have increased. This study aims to determine the influence of the yield strength on the normalized ultimate capacity (σ_{ult}/f_y) for the stiffened and unstiffened hollow steel columns. The numerical simulations were carried out for yield strength equal to (240, 360, 460, 560, and 779 MPa). Figures (28, 29, and 30) show the results for the normalized ultimate capacity (σ_{ult}/f_y) versus the ratio (B/t). From Figures 28, 29, and 30, it is shown that for all unstiffened and stiffened columns, the columns with low yield strength have a higher local buckling (B/t) limit. This is true for all the design codes, for example ANSI/AISC 360-16, referring to Equations 10, 11, and 12, the limiting values λ_p and λ_r are inversely proportional to the yield strength. Moreover, the columns with low yield strength have a lower ultimate capacity but with higher normalized ultimate capacity (σ_{ult}/f_y). This is because the local buckling occurs faster in sections with higher yield strength.

**Figure 28: Effect of yield strength on the normalized ultimate capacity (σ_{ult}/f_y) for unstiffened sections****Figure 29: Effect of yield strength on the normalized ultimate capacity (σ_{ult}/f_y) for the stiffened sections with one stiffener, where $h_s = 35$ mm****Figure 30: Effect of yield strength on the normalized ultimate capacity (σ_{ult}/f_y) for the stiffened sections with two stiffeners, where $h_s = 35$ mm**

4.3.5 Failure Modes

For hollow short steel columns, using the linear buckling analysis the steel tube was undamaged and deformations were insignificant. While, by using the non-linear buckling analysis, the effect of stiffener on the column ultimate capacity and failure modes can be figured out. The local buckling mode is plotted in form

of deformations and stresses at the instant of collapse. This is done to confirm that the buckling response is physical and that the square hollow steel columns have in real collapsed. The ultimate capacity and the stress versus strain curve of model is the main output of the non-linear analysis. Figure 31 shows the buckling modes for the US-4, SS-4, and DS-4 specimens, respectively. The stiffeners can effectively constrain the local buckling of the steel tube. Finally, the buckling of the steel tube is less obvious with the increasing of the number of stiffeners, and the stiffened steel columns have greater serviceability advantages compared to those unstiffened columns.



(a) The (US-4) specimen, (b) The (SS-4) specimen, (c) The (DS-4) specimen

Figure 31: The nonlinear local buckling modes for the stiffened and unstiffened columns

For long steel columns, the unstiffened compact sections with ($b_e/b = 1$), width-to thickness ratio ($B/t = 12.5$), and KL_e/r from 31 to 95 failed mainly due to the global buckling without any local buckling. As well as when $KL_e/r < 31$, the columns failed due to the full plastic strength, as summarized in Table 13. For the stiffened sections with one stiffener with the tube thickness $t = 20 \text{ mm}$ and the KL_e/r from 44 to 99 collapsed due to the global buckling only without any local buckling. Also, when $(KL_e)/r < 44$ the columns failed due to the full plastic strength, as summarized in Table 12. The numerical specimens for unstiffened sections with width-to thickness ratio $B/t = 50$ and KL_e/r from 30 to 80 failed by both global and local buckling (G and L) as summarized in Table 14. In addition, these columns failed due to the global buckling when $KL_e/r > 80$. For stiffened sections with one stiffener, when the columns with ($B/t = 50$) and $KL_e/r < 30$ failed by predominantly local buckling (L). When $30 < KL_e/r < 51$, the columns are in transitional mode between local and global buckling, so, the failure occurs due to a combination between these modes, as summarized in Table 15. The buckling mode for the (US-5-4000) and (US-5-7000) specimens is shown in Figure 35 and Figure 36, respectively.

4.3.6 Effect of the Stiffener Length for Short Columns

To improve the embedment of stiffened hollow steel columns, A study has been done on the performance of these columns, by studying the different stiffeners lengths. The effect of stiffener length on the stiffened sections with one and two stiffeners is shown in Figure 32 and Figure 33. According to these curves, there are three different stages could be realized. The first stage for example in Figure 32 where $B/t = 32$ and $h_s/B < 0.2$ when h_s/B increases σ_{ult}/f_y increases too. In this stage, the stiffeners and the plate may be collapsed at the same time. This is because the moment of inertia for the stiffeners and the plate is small. The second stage shows the optimum stiffeners length. At the third stage, when h_s/B increases σ_{ult}/f_y decreases. This is because the stiffeners are collapsed due to local buckling.

The optimum stiffener length at different tube thicknesses is calculated using Eq. (17) and Eq. (18) for the stiffened columns with one (SS) and two (DS) stiffeners, respectively. The (B/t) ratio, the (h_s/B) ratio, and the finite element normalized stress results are shown in Table 10 and Table 11.

$$\frac{h_s}{B} = 0.005t^2 - 0.02t + 0.14 \quad (17)$$

$$\frac{h_s}{B} = 0.005t^2 - 0.05t + 0.32 \quad (18)$$

Table10. FE normalized ultimate capacity results for stiffened columns with one stiffener, where $f_y = 779 \text{ MPa}$

| $\frac{B}{t}$ | $\frac{h_s}{B}$ | | | | | |
|---------------|--------------------|------|------|------|------|------|
| | 0.04 | 0.08 | 0.12 | 0.16 | 0.2 | 0.24 |
| | σ_{ult}/f_y | | | | | |
| 250 | 0.20 | 0.26 | 0.30 | 0.32 | 0.31 | 0.25 |
| 167 | 0.27 | 0.34 | 0.39 | 0.41 | 0.40 | 0.35 |
| 125 | 0.33 | 0.41 | 0.47 | 0.50 | 0.49 | 0.45 |
| 78 | 0.46 | 0.56 | 0.63 | 0.67 | 0.66 | 0.62 |
| 48 | 0.63 | 0.76 | 0.85 | 0.89 | 0.91 | 0.83 |
| 32 | 0.84 | 0.99 | 1.00 | 1.00 | 1.00 | 1.00 |
| 25 | 0.99 | 1.00 | 1.00 | 1.00 | 1.00 | 1.00 |
| 16 | 1.00 | 1.00 | 1.00 | 1.00 | 1.00 | 1.00 |

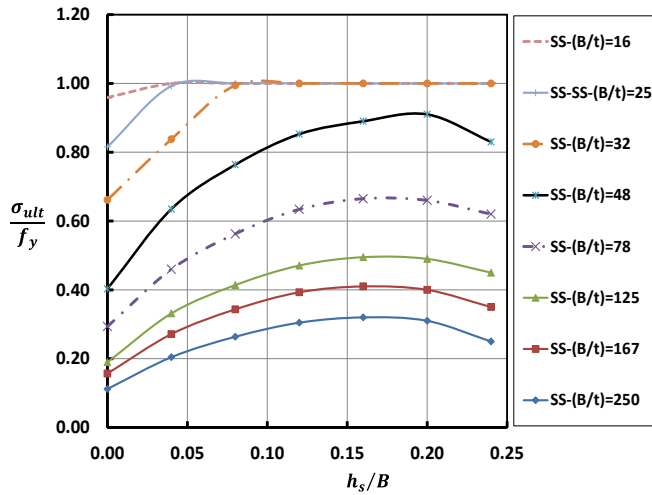


Figure 32: Effect of the stiffeners' length on the stiffened sections with one stiffener, where $f_y = 779 \text{ MPa}$

Table11. the FE normalized ultimate capacity results for stiffened columns with two stiffeners, where $f_y = 779 \text{ MPa}$

| $\frac{B}{t}$ | h_s/B | | | | | |
|---------------|--------------------|------|------|------|------|------|
| | 0.04 | 0.08 | 0.12 | 0.16 | 0.2 | 0.24 |
| | σ_{ult}/f_y | | | | | |
| 125 | 0.40 | 0.55 | 0.63 | 0.64 | 0.66 | 0.68 |
| 78 | 0.51 | 0.68 | 0.76 | 0.78 | 0.80 | 0.78 |
| 48 | 0.63 | 0.79 | 0.88 | 0.89 | 0.91 | 0.89 |
| 32 | 0.83 | 0.93 | 0.99 | 1.00 | 1.00 | 1.00 |
| 25 | 0.91 | 0.98 | 1.00 | 1.00 | 1.00 | 1.00 |
| 16 | 0.96 | 1.00 | 1.00 | 1.00 | 1.00 | 1.00 |

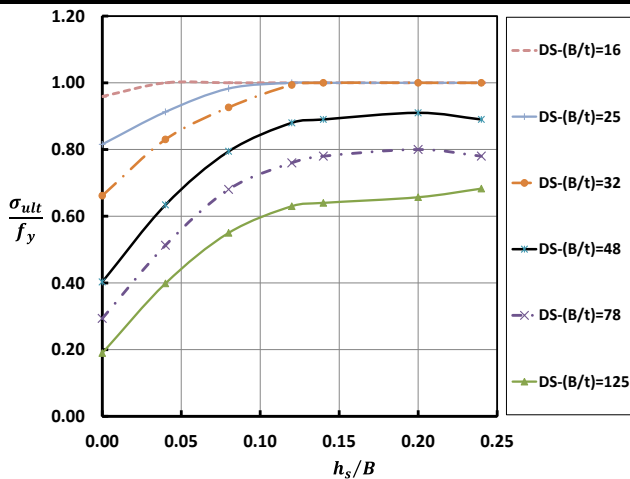


Figure 33: Effect of the stiffeners' length on the stiffened sections with two stiffeners, where yield strength $f_y = 779 \text{ MPa}$

4.3.7 The Stiffeners Effect on Long Columns

Figure 34 shows the comparison between normalized ultimate capacity (σ_{ult}/f_y) for the stiffened and unstiffened sections obtained from FEA results, where the tube thickness $t = 20 \text{ mm}$ and $t = 5 \text{ mm}$. The measured normalized ultimate capacity (σ_{ult}/f_y) for these columns is summarized in Tables (12 to 15). For

the compact unstiffened sections when $t = 20 \text{ mm}$ and $KL_e/r \leq 29$, $\sigma_{ult}/f_y = 1$ this means that the steel columns mainly collapsed due to the full plastic strength. In addition, when $KL_e/r > 29$ the $\sigma_{ult}/f_y < 1$ this means that the steel columns mainly failed due to global buckling. Similarly, for stiffened sections with one stiffener when $t = 20 \text{ mm}$ and $KL_e/r \leq 33$, the $\sigma_{ult}/f_y = 1$ this means the columns failed due to the full plastic strength. Moreover, when $KL_e/r > 29$ the $\sigma_{ult}/f_y < 1$ this means the columns failed due to global buckling. The ultimate capacity curves for the stiffened and unstiffened sections, when $t = 20 \text{ mm}$ are very close. In case of the slender sections when $t = 5 \text{ mm}$ the measured normalized ultimate capacity (σ_{ult}/f_y) is equal to 0.43 and 0.92 for unstiffened and stiffened short columns, respectively. The ultimate capacity values for stiffened sections are higher than unstiffened sections for all KL_e/r values as shown in Figure 34. According to this study, the stiffeners greatly improve the ultimate capacity of slender sections in the long columns.

Table12. The FE results of the stiffened sections with one stiffener, where the ratio $(B/t) = 12.5$

| No. | Specimen label | B/t | $\frac{KL_e}{r}$ | $\frac{\sigma_{ult}}{f_y}$ | Buckling mode |
|-----|----------------|-------|------------------|----------------------------|---------------|
| 1 | SS-20-3000 | 12.5 | 33.1 | 1.00 | Plastic |
| 2 | SS-20-4000 | 12.5 | 44.1 | 0.84 | Global |
| 3 | SS-20-5000 | 12.5 | 55.1 | 0.67 | Global |
| 4 | SS-20-6000 | 12.5 | 66.2 | 0.52 | Global |
| 5 | SS-20-7000 | 12.5 | 77.2 | 0.39 | Global |
| 6 | SS-20-8000 | 12.5 | 88.2 | 0.31 | Global |
| 7 | SS-20-9000 | 12.5 | 99.2 | 0.25 | Global |

Table13. The FE results of the unstiffened sections, where the ratio $(B/t) = 12.5$

| No. | Specimen label | B/t | $\frac{KL_e}{r}$ | $\frac{\sigma_{ult}}{f_y}$ | Buckling mode |
|-----|----------------|-------|------------------|----------------------------|---------------|
| 1 | US-20-2750 | 12.5 | 29.2 | 1.00 | Plastic |
| 2 | US-20-3000 | 12.5 | 31.8 | 0.95 | Global |
| 3 | US-20-4000 | 12.5 | 42.4 | 0.86 | Global |
| 4 | US-20-5000 | 12.5 | 53 | 0.73 | Global |
| 5 | US-20-6000 | 12.5 | 63.7 | 0.56 | Global |
| 6 | US-20-7000 | 12.5 | 74.3 | 0.43 | Global |
| 7 | US-20-8000 | 12.5 | 84.9 | 0.34 | Global |

Table14. The FE results of the unstiffened sections, where the ratio $(B/t) = 50$

| No. | Specimen label | B/t | $\frac{KL_e}{r}$ | $\frac{\sigma_{ult}}{f_y}$ | Buckling mode |
|-----|----------------|-------|------------------|----------------------------|---------------|
| 1 | US-5-3000 | 50 | 30 | 0.43 | Local |
| 2 | US-5-4000 | 50 | 40 | 0.42 | L+G |
| 3 | US-5-5000 | 50 | 50 | 0.41 | L+G |
| 4 | US-5-6000 | 50 | 60 | 0.39 | L+G |
| 5 | US-5-7000 | 50 | 70 | 0.37 | L+G |
| 6 | US-5-8000 | 50 | 80 | 0.33 | L+G |
| 7 | US-5-9000 | 50 | 90 | 0.29 | Global |

Table15. The FE results of the stiffened sections with one stiffener, where the ratio $(B/t) = 50$

| No. | Specimen label | B/t | $\frac{KL_e}{r}$ | $\frac{\sigma_{ult}}{f_y}$ | Buckling mode |
|-----|----------------|-------|------------------|----------------------------|---------------|
| 1 | SS-5-1000 | 50 | 10.3 | 0.92 | Local |
| 2 | SS-5-2000 | 50 | 20.6 | 0.87 | Local |
| 3 | SS-5-3000 | 50 | 30.9 | 0.84 | Local |
| 4 | SS-5-4000 | 50 | 41.2 | 0.75 | L+G |
| 5 | SS-5-5000 | 50 | 51.5 | 0.67 | L+G |
| 6 | SS-5-6000 | 50 | 61.8 | 0.57 | Global |
| 7 | SS-5-7000 | 50 | 72.1 | 0.45 | Global |
| 8 | SS-5-8000 | 50 | 82.4 | 0.35 | Global |

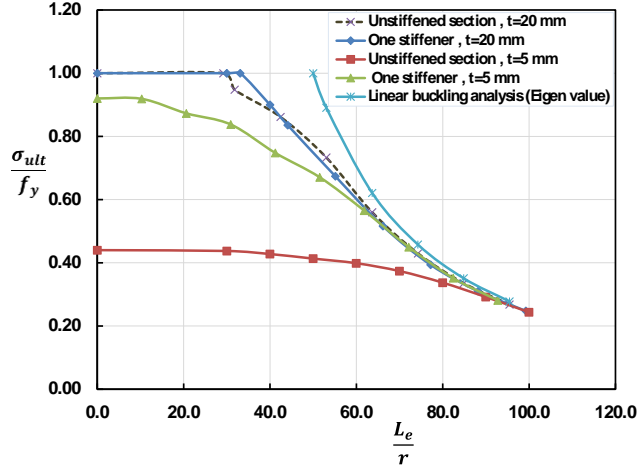


Figure 34: Comparison of the current FE results for the unstiffened and stiffened columns, where the tube thickness $t = 20mm$ and $t = 5mm$

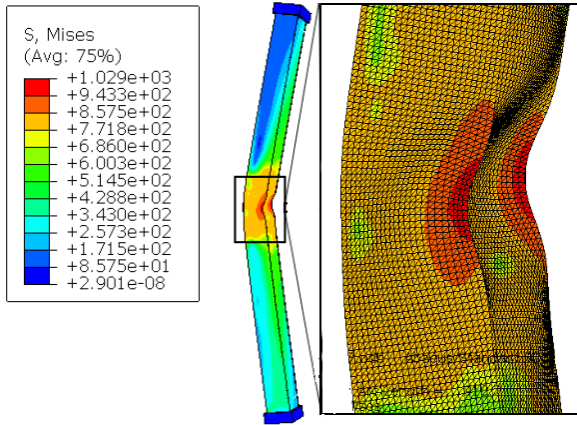


Figure 35: The buckling mode for the (US-5-4000) specimen

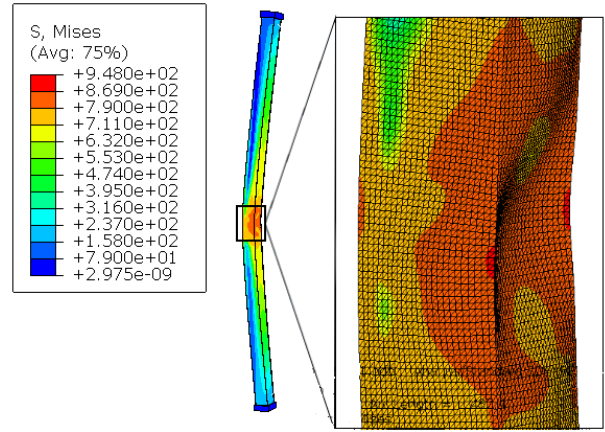


Figure 36: The buckling mode for the (US-5-7000) specimen

5 DEVELOPMENT OF NOVEL ANALYTICAL EQUATIONS

As a major result of the conducted analysis, novel equations to calculate the steel tube ultimate capacity with either one or two stiffeners was presented. The proposed equations were deduced from the parametric study using data regression analysis. The strength ratio σ_{ult}/f_y , for hollow square sections stiffened with one stiffener can be calculated using Eq. (19). The α_y and α_{hs} are strength reduction factors according to the yield strength and stiffeners length, respectively. The values of α_y and α_{hs} are determined from the results shown in Figure 29 and Figure 32.

$$\frac{\sigma_{ult}}{f_y} = \frac{7672}{779} \left(\frac{B}{t}\right)^{-0.62} + \alpha_{hs} + \alpha_y \quad (19)$$

Where; $\sigma_{ult}/f_y \leq 1$.

The reduction factors can be calculated as follows:

$$\alpha_y = 0.36 - 0.36 \sqrt{\frac{f_y}{779}} \quad (20)$$

$$\alpha_{hs} = \left(-106.92 \left(\frac{h_s}{B}\right)^2 + 35.95 \frac{h_s}{B} - 2.88\right) \left(\frac{B}{t}\right)^{-0.472} \quad (21)$$

Furthermore, the strength ratio, σ_{ult}/f_y , for hollow steel sections stiffened with two stiffeners can be calculated using Eq. (22). Where β_y and β_{hs} are strength reduction factors according to the yield strength and stiffeners length, respectively. The value of β_y and β_{hs} are determined from the parametric study, as shown in Figure 30 and Figure33.

$$\frac{\sigma_{ult}}{f_y} = \left(\frac{909}{779} \times e^{-\frac{4B}{1000t}}\right) + \beta_{hs} + \beta_y \quad (22)$$

Where $\sigma_{ult}/f_y \leq 1$

The reduction factors can be calculated as follows:

$$\beta_y = \sqrt{\frac{f_y}{779} \left(0.13 - 0.0027 \frac{B}{t} \right) + 0.0027 \frac{B}{t} - 0.16} \quad (23)$$

If $\frac{B}{t} < 53$ β_{hs} can be calculated as follows

$$\beta_{hs} = \left(-0.11 \left(\frac{h_s}{B} \right)^2 + 0.04 \frac{h_s}{B} - 0.004 \right) \left(\frac{B}{t} \right)^{1.25} \quad (24)$$

And when $\frac{B}{t} \geq 53$

$$\beta_{hs} = \left(-23 \left(\frac{h_s}{B} \right)^2 + 8 \frac{h_s}{B} - 0.75 \right) e^{-\frac{4B}{1000t}} \quad (25)$$

The comparison between the proposed strength prediction equations and experimental test results (Tao et al. [2]) for the (SS25) was conducted to verify of these equations ($\sigma_{eq}/\sigma_{test}$) = 0.97. Where the yield strength $f_y = 234.3 \text{ MPa}$, the column width $B = 250 \text{ mm}$, and the stiffeners length $h_s = 35 \text{ mm}$. Furthermore, the comparison between the proposed strength prediction equations and current (FE) results for the stiffened sections with one stiffener shown in Figure 37. Where the yield strength $f_y = 360 \text{ MPa}$, the column width $B = 250 \text{ mm}$, and the stiffeners length $h_s = 35 \text{ mm}$.

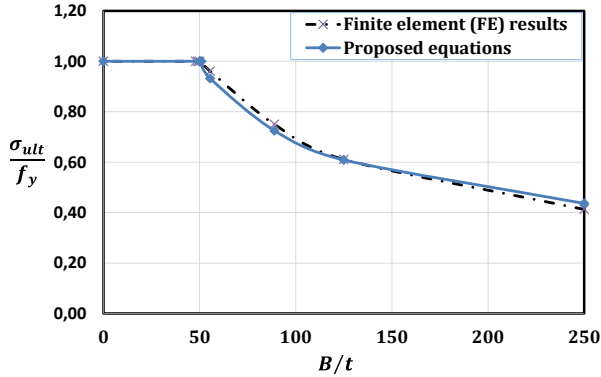


Figure 37: A Comparison between the proposed strength prediction equations and current (FE) results for the stiffened sections with one stiffener

6 CONCLUSIONS

This research aims to predict the behavior of hollow steel columns under monotonic loads and determine the effect of the main parameters on ultimate capacity. based on the study of verification, a parametric investigation was carried out to create three-dimensional finite element models that simulate the stiffened and unstiffened hollow steel columns under axial compression loads. These models focused on both the local and global buckling and were divided into two cases. Case 1, study effect of the local buckling on the ultimate capacity and behavior for stiffened and unstiffened hollow steel short columns.

Case 2, study the stiffeners effect on the steel tube ultimate capacity for long columns. The non-linear finite element (FE) analysis is used in the study to understand the effect of main structural parameters such as KL_e/r , stiffener length, the ratio of width-to-thickness B/t , and the yield stress on the hollow steel column performance. The conclusions that can be drawn are as follows:

1. The simulation of the behavior of hollow square columns using (FE) analysis can be done with about (1:3)% degree of accuracy. In addition, the (FE) analysis can reduce cost and time when compared with experimental work. The idealized elastic-plastic material model of the steel tube and the actual material models, as well as the actual initial imperfections and manufacturing errors in the real columns employed in experimental studies, were the main causes of the insignificant variations between the FEA results and experimental testing.
2. The study was conducted on the effect of the stiffeners length and proposed a novel equation to calculate the optimal stiffeners length in case of stiffened sections with one stiffener (SS) and stiffened sections with two stiffeners (DS) for short columns.
3. When increasing the width-to-thickness ratio (h_s/t) of stiffeners about the optimum stiffener length, the value of σ_{ult}/f_y decreases due to local buckling of the stiffener.
4. The current FE model produces good predictions of the steel box columns ultimate capacity compared with the analytical methods. For the unstiffened steel tube columns, the average variation in the ultimate capacity depending on the results from the present FE models and the effective width method by Uy [28] is about 4%. Furthermore, the average variation in the ultimate capacity obtained from present FE models and the modified (DSM) is about 6%. While for stiffened columns, the average variation is around 6% between current FE models and the effective width method by Norsok. Thus, it can be concluded that the proposed method can accurately predict the ultimate load capacity of short columns.
5. As a major result of the conducted analysis, a novel equation to calculate the ultimate capacity of box steel sections with one and two stiffeners was presented.
6. The presence of the stiffeners remarkably increases the ultimate capacity of slender sections in the long columns. But on the other hand, it has

no effect on the ultimate capacity of compact sections.

7. The unstiffened columns with the ratio of width to thickness $B/t = 50$ and KL_e/r from 30 to 80 collapsed as a consequence of the combination of global and local buckling (G and L). In addition, these columns collapsed according to the global buckling when $KL_e/r > 80$. For stiffened sections with one stiffener, when the columns with $B/t = 50$ and $KL_e/r < 30$ collapsed by the local buckling only (L). In addition, these columns collapsed as a consequence of the combination of global and local buckling (G and L) when the $30 < KL_e/r < 51$.

7 REFERENCES

- [1] L. Susanti, A. Kasai, and Y. Miyamoto, "Ultimate strength of box section steel bridge compression members in comparison with specifications," *Case Studies in Structural Engineering*, vol. 2, no. 1, pp. 16–23, 2014, doi: 10.1016/j.csse.2014.07.001.
- [2] Z. Tao, L. H. Han, and Z. Bin Wang, "Experimental behaviour of stiffened concrete-filled thin-walled hollow steel structural (HSS) stub columns," *Journal of Constructional Steel Research*, vol. 61, no. 7, pp. 962–983, Jul. 2005, doi: 10.1016/j.jcsr.2004.12.003.
- [3] M. A. Dabaon, M. H. El-Boghdadi, and M. F. Hassanein, "A comparative experimental study between stiffened and unstiffened stainless steel hollow tubular stub columns," *Thin-Walled Structures*, vol. 47, no. 1, pp. 73–81, Jan. 2009, doi: 10.1016/j.tws.2008.05.008.
- [4] B. Somodi and B. Kövesdi, "Residual stress measurements on welded square box sections using steel grades of S235–S960," *Thin-Walled Structures*, vol. 123, no. July 2016, pp. 142–154, 2018, doi: 10.1016/j.tws.2017.11.028.
- [5] M. Khan, B. Uy, Z. Tao, and F. Mashiri, "Concentrically loaded slender square hollow and composite columns incorporating high strength properties," *Engineering Structures*, vol. 131, pp. 69–89, 2017, doi: 10.1016/j.engstruct.2016.10.015.
- [6] F. Javidan, A. Heidarpour, X. L. Zhao, and J. Minkkinen, "Performance of innovative fabricated long hollow columns under axial compression," *Journal of Constructional Steel Research*, vol. 106, pp. 99–109, 2015, doi: 10.1016/j.jcsr.2014.12.013.
- [7] K. M. El-Sayed, A. S. Debaiky, N. N. Khalil, and I. M. El-Shenawy, "Improving buckling resistance of hollow structural steel columns strengthened with polymer-mortar," *Thin-Walled Structures*, vol. 137, no. November 2018, pp. 515–526, 2019, doi: 10.1016/j.tws.2018.12.029.
- [8] B. Zheng, G. Shu, F. Xie, and Q. Jiang, "Design of cold-rolled stainless steel rectangular hollow section columns," *Journal of Constructional Steel Research*, vol. 170, p. 106072, 2020, doi: 10.1016/j.jcsr.2020.106072.
- [9] M. Anbarasu and M. Ashraf, "Interaction of local-flexural buckling for cold-formed lean duplex stainless steel hollow columns," *Thin-Walled Structures*, vol. 112, no. December 2016, pp. 20–30, 2017, doi: 10.1016/j.tws.2016.12.006.
- [10] M. Nassirnia, A. Heidarpour, X. L. Zhao, and J. Minkkinen, "Innovative hollow columns comprising corrugated plates and ultra high-strength steel tubes," *Thin-Walled Structures*, vol. 101, pp. 14–25, 2016, doi: 10.1016/j.tws.2015.12.020.
- [11] M. Longshithung Patton and K. Darunkumar Singh, "Buckling of fixed-ended lean duplex stainless steel hollow columns of square, L-, T-, and +-shaped sections under pure axial compression - A finite element study," *Thin-Walled Structures*, vol. 63, pp. 106–116, 2013, doi: 10.1016/j.tws.2012.09.003.
- [12] N. Schillo and M. Feldmann, "Interaction of local and global buckling of box sections made of high strength steel," *Thin-Walled Structures*, vol. 128, no. March, pp. 126–140, 2018, doi: 10.1016/j.tws.2017.07.009.
- [13] L. Pavlovčič, B. Froschmeier, U. Kuhlmann, and D. Beg, "Finite element simulation of slender thin-walled box columns by implementing real initial conditions," *Advances in Engineering Software*, vol. 44, no. 1, pp. 63–74, 2012, doi: 10.1016/j.advengsoft.2011.05.036.
- [14] E. Ellobody, "Buckling analysis of high strength stainless steel stiffened and unstiffened slender hollow section columns," *Journal of Constructional Steel Research*, vol. 63, no. 2, pp. 145–155, 2007, doi: 10.1016/j.jcsr.2006.04.007.
- [15] S. J. Hilo, S. M. Sabih, M. M. Faris, and A. W. Al-Zand, "Numerical Investigation on the Axial Load Behaviour of Polygonal Steel Tube Columns," *International Review of Civil Engineering*, vol. 13, no. 5, pp. 397–408, 2022, doi: 10.15866/irece.v13i5.20548.
- [16] T. G. Singh and K. D. Singh, "Design of perforated cold-formed steel hollow stub columns using direct strength method," *Thin-Walled Structures*, vol. 168, no. July, p. 108265, 2021, doi: 10.1016/j.tws.2021.108265.
- [17] H. Ban and Y. Mei, "Local buckling behavior behaviour of stainless-clad bimetallic steel built-up square hollow section stub columns," *Thin-Walled Structures*, vol. 182, no. July 2022, p. 110207, 2023, doi: 10.1016/j.tws.2022.110207.
- [18] J. Liu, H. Fang, and T.-M. Chan, "Numerical investigation on local buckling behaviour of cold-formed high strength steel irregular hexagonal hollow section stub columns," *Thin-Walled Structures*, vol. 185, no. March, p. 110571, 2023, doi: 10.1016/j.tws.2023.110571.
- [19] I. Arrayago, E. Real, E. Mirambell, and L. Gardner, "The Continuous Strength Method for the design of stainless steel hollow section columns," *Thin-Walled Structures*, vol. 154, no. January, p. 106825, 2020,

doi: 10.1016/j.tws.2020.106825.

doi: 10.1080/10462937.2017.1349256.

- [20] H. Ban, G. Shi, Y. Shi, and Y. Wang, "Residual stress of 460 MPa high strength steel welded box section: Experimental investigation and modeling," *Thin-Walled Structures*, vol. 64, pp. 73–82, 2013, doi: 10.1016/j.tws.2012.12.007.
- [21] X. Cao, Y. Xu, M. Wang, G. Zhao, L. Gu, and Z. Kong, "Experimental study on the residual stresses of 800 MPa high strength steel welded box sections," *Journal of Constructional Steel Research*, vol. 148, pp. 720–727, 2018, doi: 10.1016/j.jcsr.2018.06.019.
- [22] L. Jaamala, K. Mela, J. Laurila, M. Rinne, and P. Peura, "Probabilistic modelling of residual stresses in cold-formed rectangular hollow sections," *Journal of Constructional Steel Research*, vol. 189, no. December 2021, p. 107108, 2022, doi: 10.1016/j.jcsr.2021.107108.
- [23] J. R. Association, "Specifications for highway bridges, Part V," *Earthquake resistant design*, vol. 228, no. September, 1996.
- [24] A. I. of S. Construction, "Specification for Structural Steel Buildings," pp. 1–612, 2010.
- [25] N. Standard, "National Standard of the People's Republic of China Notice on Ministry of Housing and Urban-Rural Development," 2003.
- [26] L. Guo, S. Zhang, W. J. Kim, and G. Ranzi, "Behavior of square hollow steel tubes and steel tubes filled with concrete," *Thin-Walled Structures*, vol. 45, no. 12, pp. 961–973, Dec. 2007, doi: 10.1016/j.tws.2007.07.009.
- [27] A. B. B. Abu-Sena, M. Said, M. A. Zaki, and M. Dokmak, "Behavior of hollow steel sections strengthened with CFRP," *Construction and Building Materials*, vol. 205, pp. 306–320, 2019, doi: 10.1016/j.conbuildmat.2019.01.237.
- [28] B. Uy, "Local and post-local buckling of concrete filled steel welded box columns," *Journal of Constructional Steel Research*, vol. 47, no. 1–2, pp. 47–72, 1998, doi: 10.1016/S0143-974X(98)80102-8.
- [29] American Iron and Steel Institute, "AISI S100: North American Specification for the Design of Cold-Formed Steel Structural Members (with commentaries)," p. 505, 2016.
- [30] H. Fang and T. M. Chan, "Axial compressive strength of welded S460 steel columns at elevated temperatures," *Thin-Walled Structures*, vol. 129, no. March, pp. 213–224, 2018, doi: 10.1016/j.tws.2018.04.006.
- [31] Norsok-Standard, "Norsok Standard M-001," no. Rev.4, 2004.
- [32] Von Karman T, Sechler EE, Donnel LH. Strength of thin plates in compression. *Trans ASME* 1932;54:53.
- [33] Winter G. Strength of thin steel compression flanges. Reprint No. 32. Ithaca, NY, USA: Cornell University Engineering Experimental Station, 1947.
- [34] A. I. of S. Construction "Specification for Structural Steel Buildings" Q., vol. 37, no. 2, pp. 169–170, 2017,
- [35] ABAQUS. Standard user's manual, version 2017. Providence, RI (USA): Dassault Systems Corp.; 2017.